The anisotropy of magnetic susceptibility (AMS) in low-grade, cleaved pelitic rocks: influence of cleavage/bedding angle and type and relative orientation of magnetic carriers

TIMOTHY N. DEBACKER[1], PHILIPPE ROBION[2] & MANUEL SINTUBIN[3]

[1] *Structural Geology & Tectonics Group, Katholieke Universiteit Leuven, Redingenstraat 16, B-3000 Leuven, Belgium (e-mail: timothy.debacker@geo.kuleuven.ac.be)*

[2] *CNRS-UMR 7072 'Laboratoire de Tectonique', Département des Sciences de la Terre et de l'Environnement, Université de Cergy-Pontoise, Avenue du Parc-le Campus- Bat I, 95031 Cergy Pontoise, France (e-mail: philippe.robion@geol.u-cergy.fr)*

[3] *Structural Geology & Tectonics Group, Katholieke Universiteit Leuven, Redingenstraat 16, B-3000 Leuven, Belgium (e-mail: manuel.sintubin@geo.kuleuven.ac.be)*

Abstract: Cambrian and Silurian, low-grade, pelitic rocks of the single-phase deformed Brabant Massif consistently have a maximum magnetic susceptibility axis (K1) parallel to the cleavage/bedding intersection. In contrast, the minimum susceptibility axis (K3) either coincides with the bedding pole, with the cleavage pole or occupies an intermediate position. Anisotropy of anhysteretic remanence (AARM) and X-ray pole figure goniometry allow the distinguishing of the orientation distributions of the ferromagnetic and paramagnetic (white mica and chlorite) carriers, respectively. Mismatches between K3 and the poles to the macroscopic fabric elements (i.e. bedding and cleavage) are attributed to different orientations of the different magnetic (*s.l.*) carriers. A strong relationship exists between the cleavage/bedding angle and the shape parameter: low, respectively high angles leading to oblate, respectively prolate susceptibility ellipsoids. However, differences are observed between the Cambrian and Silurian samples in terms of the shape parameter and the behaviour of the degree of anisotropy with changing cleavage/bedding angle. This is tentatively attributed to differences in relative orientation and mineralogy of the magnetic (*s.l.*) carriers. These results demonstrate the influence of the relative orientation of the different carriers on AMS and suggest that, although being a petrofabric tool, AMS cannot be used as a strain gauge in the case of composite magnetic fabrics.

Because of the fine grain-size and the common scarcity of classical strain markers (deformed pebbles, macro-fossils, reduction spots, etc.), performing quantitative strain analyses in slate belts may be difficult. As an alternative, one may apply more analytical methods such as phyllosilicate X-ray pole figure goniometry (e.g. Oertel 1983; Sintubin 1994*a*, *b*; van der Pluijm *et al.* 1994) and the analysis of the anisotropy of magnetic susceptibility (e.g. Graham 1954; Fuller 1964; Rathore 1979; Hrouda 1982; Borradaile & Henry 1997 and references therein). However, although these petrofabric methods have been applied in structural geology for more than 20 years, the relationship with strain is still debated.

The anisotropy of magnetic susceptibility (AMS) in particular not only depends on the degree of deformation but is to a large extent controlled by the lithology (rock type, type of magnetic carriers, and orientation and concentration of different carriers) (e.g. Borradaile & Tarling 1981; Borradaile 1987, 1988). According to several studies, in foliated rocks, such as slates, the principal magnetic susceptibility axes reflect the tectonic foliation, with the minimum susceptibility axis (K3) perpendicular to foliation and the maximum susceptibility axis (K1) parallel to the tectonic extension direction or to the cleavage/bedding intersection (e.g. Rathore 1979; Hrouda 1982; Aubourg *et al.* 1991; Robion *et al.* 1995; Borradaile & Henry 1997; Hirt *et al.* 2000; Nakamura & Borradaile 2001; Parés & van der Pluijm 2002). Similarly, in shales, the principal magnetic susceptibility axes may reflect the bedding-parallel compaction fabric, with the minimum susceptibility axis (K3) perpendicular to bedding (e.g. Li & Powell 1993; Hirt *et al.* 1995). Such a coincidence between the pole to the macroscopic fabric

From: MARTÍN-HERNÁNDEZ, F., LÜNEBURG, C. M., AUBOURG, C. & JACKSON, M. (eds) 2004. *Magnetic Fabric: Methods and Applications*. Geological Society, London, Special Publications, **238**, 77–107. 0305-8719/04/$15.00

elements (cleavage in slate or bedding in shale) and the minimum susceptibility axis (K3) suggests that the (minimum axis of) AMS is controlled by one or more types of magnetic carriers all parallel to the macroscopic fabric elements. In such cases, a qualitative and possibly even a quantitative relationship may exist between AMS and strain (compaction strain in the case of shale, tectonic shortening strain in the case of slate).

However, a different situation occurs in rocks with two competing macroscopic fabric elements. Common examples of these are poorly deformed sedimentary rocks, characterized by both a bedding fabric and a cleavage fabric. In such rocks the maximum susceptibility axis (K1) is commonly parallel to the cleavage/bedding intersection, whereas the minimum susceptibility axis (K3) may remain perpendicular to bedding (Saint Bézar *et al.* 2002; Parés & van der Pluijm 2002), or in other cases may be perpendicular to cleavage or occupy an intermediate position in between the pole to bedding and the pole to cleavage (e.g. Robion *et al.* 1995; Lüneburg *et al.* 1999; Frizon de Lamotte *et al.* 2002). The work of Lüneburg *et al.* (1999), for instance, in which the minimum (K3) and intermediate (K2) susceptibility axes often show a girdle distribution (e.g. Housen *et al.* 1993; Parés & van der Pluijm 2003), demonstrates the competing influence of both bedding-parallel (related to sedimentation, compaction and pre-kinematic metamorphism) and cleavage-parallel (related to tectonic shortening and syn- to post-kinematic metamorphism) magnetic (*s.l.*) carriers. In such cases, in which the minimum susceptibility axis is not perpendicular to the cleavage, it is unlikely that a simple relationship will exist between finite strain and AMS (e.g. Housen *et al.* 1993; Parés & van der Pluijm 2002). Indeed, Housen *et al.* (1993), who studied the effect of composite magnetic fabrics on AMS by means of experiments and numerical models, conclude that in the presence of composite magnetic fabrics, quantitative measures of finite strain are limited by the ability to determine accurately the degree of anisotropy and relative susceptibility of each component fabric element. Housen *et al.* (1993) further conclude that in the case of two competing fabrics (1) the maximum susceptibility axis (K1) parallels the intersection axis of the two fabrics, and (2) the degree of anisotropy and shape of the susceptibility ellipsoid changes in function of the angle between the two fabrics. Although the parallelism of the maximum susceptibility axis and the cleavage/bedding intersection is well documented, we are not aware of studies demonstrating the effect of variations in angle between cleavage and bedding on AMS in natural rocks. This effect in natural rocks is documented in the present study. Moreover, an attempt is made to resolve the AMS-ellipsoid orientation qualitatively in terms of the preferred orientation of paramagnetic and ferromagnetic carriers. As will be demonstrated, even with the help of additional techniques, the AMS of rocks with composite magnetic fabrics may be difficult to interpret and therefore cannot be used as a measure of strain.

Geological setting and sampling

The largely concealed Lower Palaeozoic Brabant Massif (Fig. 1) is a typical example of a slate belt, forming the south-eastern part of the Anglo-Brabant deformation belt, one of the deformation belts of eastern Avalonia (Van Grootel *et al.* 1997; Verniers *et al.* 2002). The massif consists of low-grade, mainly fine-grained, siliciclastic deposits, ranging from the lowermost Cambrian in the core of the massif to upper Silurian along the rims. An angular unconformity separates these deformed Lower Palaeozoic deposits from overlying, diagenetic, undeformed Givetian deposits (Legrand 1967; De Vos *et al.* 1993; Van Grootel *et al.* 1997; Debacker *et al.* 1999). At present, there is only evidence for a single progressive deformation, currently considered to have taken place between the Llandovery and the end of the Early Devonian, possibly continuing into the Eifellian (Debacker 2001; Debacker *et al.* 2002). The main features associated with this deformation are folds with a well-developed, cogenetic cleavage (Sintubin 1997, 1999; Debacker 2001; Debacker *et al.* 2002; Verniers *et al.* 2002). The stratigraphy and structural architecture of the Brabant Massif are well known, making it an ideal study area for the geological application of AMS in low-grade slate belts.

Criteria used to select sampling localities are the fine grain size (only fine-grained siltstone and claystone), the homogeneity of the deposits (in order to avoid grain-size-dependent variations such as cleavage refraction), the presence of tectonic folds with a moderately to well-developed cogenetic cleavage (in order to compare magnetic fabrics with bedding and cleavage orientations around folds), a well-known structural architecture and a known degree of metamorphism. Four suitable lithostratigraphic units from three large outcrops were sampled. These are the Ripain Member and the Asquempont Member of the Lower to lower Middle

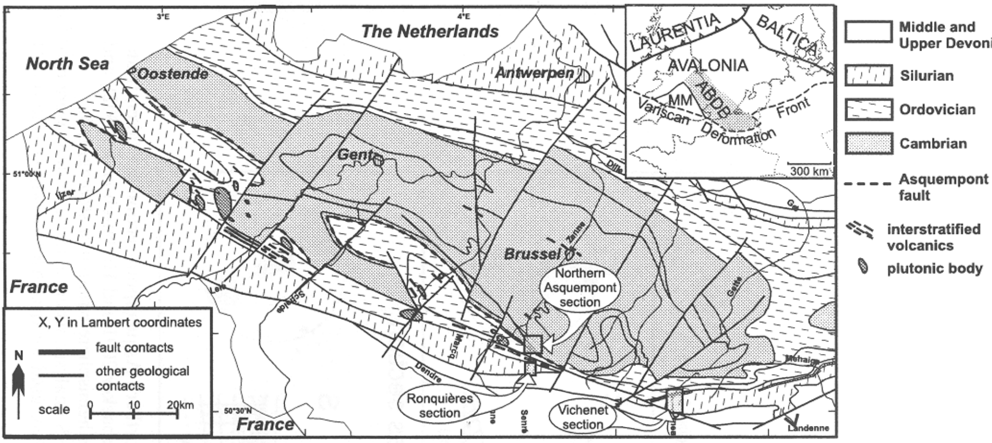

Fig. 1. Geological subcrop map of the Brabant Massif (after De Vos *et al.* 1993 and Van Grootel *et al.* 1997), showing the position of the sampled outcrops. The upper right inset shows the position of the Brabant Massif, forming the southeastern part of the Anglo-Brabant Deformation Belt (ABDB), situated within the micro-continent Avalonia along the NE-side of the Midlands Microcraton (MM).

Cambrian Oisquercq Formation in outcrop Northern Asquempont section (Sennette valley), the Wenlock Vichenet Formation in the Vichenet section (Orneau valley) and the lower Ludlow Ronquières Formation in the Ronquières section (Inclined Shiplift of Ronquières, Sennette valley) (Figs 1 & 2). All the sampled lithologies are homogeneous mudstone, mainly composed of white mica, chlorite and quartz, with a minor amount of dispersed opaque material (cf. Geerkens & Laduron 1996). All the sampled lithologies underwent an anchizonal degree of metamorphism, as suggested by illite crystallinity studies (Geerkens & Laduron 1996; Van Grootel *et al.* 1997) and the cleavage is moderately developed, corresponding to the embryonic cleavage stage to cleavage stage of Ramsay & Huber (1983).

The Ripain Member, representing the lower member of the Lower to lower Middle Cambrian Oisquercq Formation, consists of blue-grey to purplish grey, extremely homogeneous fine-grained mudstone (Verniers *et al.* 2001). The samples used in this study were taken from outcrop Northern Asquempont section (Figs 1 & 2). In this outcrop steeply plunging tectonic folds occur, with a Z-shaped geometry and a predominance of sub-vertical to steeply ENE-dipping, WSW-ward younging limbs (Debacker 2001; Debacker *et al.* 2004). The rocks are affected by a moderately to well-developed cleavage, cogenetic with the folds. Microscopic observations show that white mica, oriented parallel to cleavage, is present throughout the rock mass. Occasionally, vague cleavage-parallel alignments of opaque material, resembling cleavage domains, reflect a spaced cleavage. A spaced cleavage becomes apparent locally around chlorite/mica stacks and opaque objects. Chlorite/mica stacks occur sub-parallel to bedding, as well as sub-parallel to cleavage (Debacker 2001).

The Asquempont Member represents the upper member of the Lower to lower Middle Cambrian Oisquercq Formation. It consists of rather porous, greenish grey to green, very homogeneous mudstone, occasionally with laminated siltstone. In outcrop Northern Asquempont section this member contains folds with variable plunges, ranging from sub-horizontal to steeply plunging, which are cogenetic with the cleavage (Fig. 2; Debacker 2001; Debacker *et al.* 2004; cf. Sintubin *et al.* 1998). The cleavage is only moderately developed, often having an irregular, anastomosing nature. Microscopically, cleavage is mainly reflected by white mica, distributed throughout the rock mass and oriented parallel to cleavage. A spaced cleavage, reflected by vague bands of opaque material, is only apparent around chlorite/mica stacks. Chlorite/mica stacks occur sub-parallel to both bedding and cleavage (Debacker 2001).

The Vichenet Formation (Wenlock, Silurian) consists of grey mudstone, siltstone and fine sandstone, often with calcareous pelite, forming an alternation of distal thick-bedded turbidites, characteristically Tde-sequences (for turbidite terminology see Bouma 1962), and thin-bedded laminated hemipelagites (De Schepper 2000;

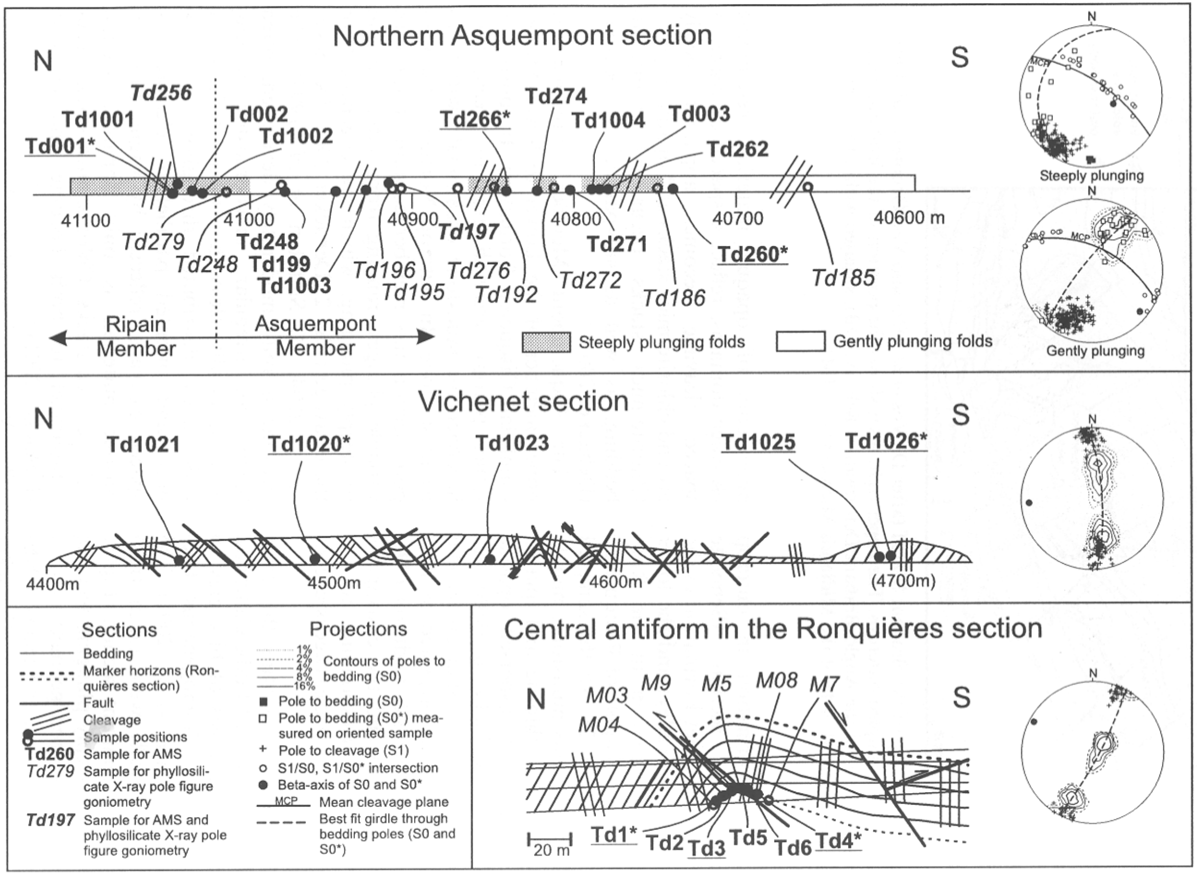

Fig. 2. Sample positions within, and structural architecture of, the three sampled outcrops. Structural data from the Northern Asquempont section are taken from Debacker (2001) and Debacker *et al.* (2004), those from the Vichenet section are taken from Belmans (2000; see also Debacker 2001 and Herbosch *et al.* 2002), and those from the central antiform within the Inclined Shiplift of Ronquières are taken from Debacker *et al.* (1999). Lower-hemisphere equal-area stereographic projections are added showing bedding, cleavage and cleavage/bedding intersections. Samples in bold were used for AMS analysis, whereas those in italic were used for phyllosilicate X-ray pole figure goniometry. Samples in bold and italic were used for both. Underlined (bold) samples were used for (p)AARM analyses, and (bold) samples marked by * were heated in the oven in order to determine the ferromagnetic mineralogy.

Verniers *et al.* 2001). Samples were taken from the type-section of this formation, the Vichenet section in the Orneau valley (Figs 1 & 2). Only the most fine-grained, homogeneous interval was sampled, being the homogeneous, pelitic e-interval (cf. Bouma 1962). The type-section contains sub-horizontal to gently plunging open folds, affected by a well-developed cogenetic cleavage, showing a pronounced convergent cleavage fanning with a symmetrical disposition with respect to the fold hinges (Fig. 2; Belmans 2000; Herbosch *et al.* 2002). Microscopically, the cleavage has an anastomosing disjunctive nature in the sampled intervals. The width of the microlithons ranges from 10 to 30 μm, whereas the cleavage domains, with a high concentration of opaque material, are generally 5 to 10 μm wide. Chlorite, as a part of chlorite-mica stacks, generally occurs in the microlithons, whereas white mica, oriented parallel to cleavage, is abundant in the cleavage domains (Belmans 2000; Debacker 2001).

The Ronquières Formation (lower Ludlow, Silurian) consists of grey mudstone, siltstone and fine sandstone, forming an alternation of distal turbidites, predominantly Tcde-intervals (for turbidite terminology see Bouma 1962), and laminated hemipelagites (Louwye *et al.* 1992; Verniers *et al.* 1992, 2001). Samples were taken from the type-section of this formation, the Ronquières section in the Inclined Shiplift of Ronquières, Sennette valley (Figs 1 & 2). Also here, only the most fine-grained, homogeneous, interval was sampled, being the pelitic e-interval. Because of the availability of turbidite logs and at least two marker horizons (Verniers *et al.* 1992), it was possible to sample a single bed across a large antiform occupying a central position within the section (Fig. 2). The sampled bed is the e-interval of turbidite sequence 121 of Verniers *et al.* (1992), situated between 30 and 65 cm below the lower marker horizon depicted in Figure 2. The sampled antiform has a gentle to open interlimb angle, a sub-horizontal to gentle plunge and a well-developed cogenetic cleavage, showing a convergent cleavage fanning with a symmetrical disposition with respect to the fold hinge (Legrand 1967; Debacker *et al.* 1999). Microscopically, the cleavage has a spaced nature, with microlithons in the order of 10 to 30 μm wide. White mica is mainly concentrated in the cleavage domains, aligned sub-parallel to cleavage, whereas chlorite, as a part of chlorite/mica stacks, is mainly concentrated in the microlithons, usually statistically aligned sub-parallel to bedding. Opaque material is usually concentrated in the cleavage domains. It is not clear whether cleavage is a disjunctive or a crenulation type cleavage (Debacker *et al.* 1999; Debacker 2001).

Methodology

Magnetic anisotropy studies

The vast majority of the investigated samples consists of oriented hand specimens (e.g. TD001) that were cut into cubes, on average 7 per sample (cf. Table 1), with size $2 \times 2 \times 2$ cm (e.g. TD001a, TD001b, etc.). Only in four cases (TD1001, TD1002, TD1003, TD1004) was sampling performed by means of a hand drill, giving cylinders with a diameter of 2.4 cm and 2.1 cm high. The reason for the small number of drill core samples with respect to hand specimen cubes is the presence of the cleavage, along which the rocks tend to break during drilling. Broken samples, both cubes and cylinders, were glued together using a non-magnetic glue. There are no significant differences in results between the cylinders and the cubes, neither between the intact samples and the samples that were glued together again.

The anisotropy of the low field susceptibility (AMS) and of the remanent magnetization (AARM) were investigated, the former at Katholieke Universiteit Leuven (Belgium), the latter at Cergy-Pontoise University (France). Whereas the anisotropy of magnetic susceptibility (AMS) represents the contribution of all magnetic constituents of a rock, anisotropy of anhysteretic remanent magnetization (AARM) only reflects the ferromagnetic fraction without paramagnetic and diamagnetic contributions. Hence, AMS and AARM have different sources, and combining these two methods may give complementary information in cases where sources of magnetization are complex (McCabe *et al.* 1985).

AMS was measured with a KLY3S Kappabridge (Jelínek & Pokorný 1997) at Katholieke Universiteit Leuven. The susceptibility tensor is computed by using the device software. The eigenvectors of this tensor, K1, K2 and K3, corresponding to the maximum, intermediate and minimum susceptibility, respectively, reflect the orientation and shape of the magnetic ellipsoid. Three different arrangements of the eigenvectors K1, K2 and K3 are used: the corrected degree of anisotropy Pj (Jelínek 1981), the shape parameter T (Jelínek 1981) and the mean susceptibility Km (cf. Borradaile 1988; Tarling & Hrouda 1993). To investigate the effects of mineralogy on the susceptibility anisotropy, Pj and Km are compared. The effect of the ferromagnetic fraction on Pj is generally accompanied by an increase of Km, and on a Pj/Km plot the paramagnetic contribution has an upper limit around Pj ~1.2–1.3 and Km ~300–500 × 10^{-6} SI (Rochette 1987*a*; Rochette *et al.* 1992; Martín-Hernández & Hirt 2003). Also the shape parameter T and the degree of anisotropy Pj are compared. Whereas Pj reflects the degree of preferred orientation of magnetic minerals (*s.l.*), T is a measurement of the shape of the ellipsoid. If $-1 < T < 0$, the susceptibility ellipsoid is prolate, whereas if $0 < T < 1$, the susceptibility ellipsoid is oblate (Jelínek 1981). The AMS data, averaged per sample, are summarized in Table 1.

AARM is based on the ability of samples to acquire a remanent magnetization when an alternating field is applied in the presence of a small direct field (McCabe *et al.* 1985). Magnetization is imparted along a chosen direction of the sample in an alternating field peak of 100 mT with a coaxial small direct field of 100 μT. Before processing magnetization, the sample is demagnetized with an alternating field of 100 mT. Both the magnetization and demagnetization procedures are performed by the LAD-3 AF device manufactured by AGICO. After each magnetization step the sample is measured with a JR5 spinner magnetometer. The AARM tensor is determined by using the Jelínek procedure (Jelínek 1993) that had been developed for characterizing the anisotropy of isothermal remanent magnetization. In this procedure, 12 senses (6 directions) of magnetization are used, with the first and second sense opposed (same direction), the third and fourth opposed and so forth. This measuring scheme is useful when a hard coercivity component of magnetization cannot be demagnetized with a 100 mT alternating field. The remanibility tensor R is constructed in the same way as the susceptibility tensor K, by means of the least square inversion method. By combining principal remanibility values R1, R2, R3 (with R1 > R2 > R3) we obtain the anisotropy degree Pj_R and the shape parameter T_R. Because of the maximum value of the alternating field applied, the main minerals controlling AARM are magnetite, with wide range of coercivities, and low-coercivity pyrrhotite. In addition, on a few selected samples we measured partial AARM (pAARM). This method consists of imparting an anhysteretic magnetization in a selected window between two specified values of alternating field, in the presence of a 100 μT direct field. On the basis of coercivity spectra of the samples, we chose two windows, the first between 0 and 50 mT and the second between 50 and 100 mT (cf. Jackson *et al.* 1988).

Magnetic mineralogy

Ferromagnetic mineralogy was investigated by applying a stepwise demagnetization of a 'three axis' isothermal remanent magnetization following the procedure described by Lowrie (1990). This coercivity/blocking temperature spectrum analysis separates ferromagnetic minerals with different magnetic properties. We applied three successive saturation fields (1.4 T, 0.6 T and 0.12 T) along three perpendicular directions on the samples. These are then demagnetized thermally in steps of 50 °C, with finer steps around 325 °C and 580 °C, the Curie temperatures of pyrrhotite and magnetite respectively. Samples were heated up to 700 °C. During this stepwise demagnetization, bulk magnetic susceptibility was monitored with a KLY3S at room temperature in order to detect artificial changes in magnetic properties due to heating

X-ray pole figure goniometry

Mica (001) ($d = 10$ Å) and chlorite (002) ($d = 7$ Å) orientation distributions were measured by means of an X-ray pole figure goniometer. Pole figure measurements were performed using Fe-filtered Co-radiation (40 kV × 30 mA). Complete normalized pole figures were obtained by combining incomplete pole figure measurements, performed in transmission mode, on two mutually perpendicular sections of the sample, both perpendicular to the main foliation (bedding or cleavage). A more extensive description of the procedure can be found in Sintubin *et al.* (1995). The phyllosilicate preferred orientations are evidenced using contoured orientation distributions (lower-hemisphere equal-area projections). Contours represent 'multiples of a random distribution' (m.r.d.). The interpretation of the pole figures is based, on the one hand, on the pole figure patterns (Sintubin 1994*a*, *b*, 1998), taking into account the symmetry of the orientation distribution and its angular relationship with distinct fabric elements (bedding, cleavage, etc.), and, on the other hand, on the degree of preferred orientation.

Ferromagnetic mineralogy

An apparent relationship exists between the ferromagnetic mineralogy and the stratigraphy (Fig. 3). The ferromagnetic mineralogy of the Ripain Member of the Oisquercq Formation is dominated by hematite (blocking temperature

Table 1. *Main parameters of the investigated samples, averaged over the measured specimens (cubes, cylinders)*

Sample	n	K1	K2	K3	95% confidence E12/E23/E13	Lineation L	Foliation F	Angle S0–S1	Shape parameter T	Degree of anisotropy Pj	Mean suscept.
Ripain Member, Oisquercq Formation (Lower to lower Middle Cambrian), Asquempont section, Sennette valley											
TD1001	7	1.0924	1.0629	0.8448	8.14/0.97/0.87	1.0279	1.2583	16	0.7867 ± 0.1123	1.4315 ± 0.0265	407.1 ± 20.5
TD1002	9	1.0932	1.0534	0.8534	4.81/0.91/0.72	1.0379	1.2344	25	0.7011 ± 0.1110	1.4016 ± 0.0228	415.9 ± 33.7
TD001	6	1.0972	1.0598	0.8430	23.33/4.07/3.48	1.0353	1.2574	16	0.7354 ± 0.0611	1.4369 ± 0.0308	401.5 ± 7.6
TD002	5	1.0671	1.0539	0.8790	16.62/1.30/1.20	1.0126	1.1990	25	0.8714 ± 0.0173	1.3232 ± 0.0173	386.8 ± 10.5
TD256	7	1.1167	1.0497	0.8336	12.60/4.83/3.43	1.0640	1.2594	26	0.5755 ± 0.1242	1.4631 ± 0.0378	375.9 ± 6.3
Asquempont Member, Oisquercq Formation (Lower to lower Middle Cambrian), Asquempont section, Sennette valley											
TD1003	13	1.0506	1.0150	0.9344	0.95/0.47/0.33	1.0351	1.0863	55	0.4109 ± 0.0356	1.1604 ± 0.0161	339.7 ± 14.3
TD1004	6	1.0466	1.0193	0.9342	5.08/1.50/1.07	1.0269	1.0911	25	0.5349 ± 0.0856	1.1626 ± 0.0097	431.9 ± 23.4
TD003	9	1.0469	1.0297	0.9235	15.56/2.48/2.11	1.0167	1.1150	25	0.7350 ± 0.0691	1.1932 ± 0.0133	327.4 ± 8.2
TD260	7	1.0560	1.0214	0.9226	7.53/2.60/1.96	1.0339	1.1071	39	0.5056 ± 0.0348	1.1934 ± 0.0080	358.2 ± 19.1
TD262	8	1.0441	1.0230	0.9329	7.96/1.98/1.59	1.0207	1.0966	18	0.6331 ± 0.0599	1.1670 ± 0.0218	381.1 ± 37.5
TD274	6	1.0322	0.9939	0.9739	3.70/6.98/2.43	1.0384	1.0206	71	−0.2965 ± 0.0620	1.0755 ± 0.0046	437.6 ± 22.8
TD266	5	1.0453	0.9985	0.9562	13.04/14.80/7.02	1.0468	1.0443	86	−0.0298 ± 0.1108	1.1036 ± 0.0119	335.2 ± 9.9
TD199	9	1.0576	1.0139	0.9285	12.12/7.19/4.47	1.0431	1.0920	50	0.3594 ± 0.1323	1.1732 ± 0.0093	318.4 ± 18.3
TD271	6	1.0494	1.0266	0.9240	9.67/2.18/1.78	1.0222	1.1111	13	0.6533 ± 0.0467	1.1913 ± 0.0124	333.0 ± 6.7
TD197	6	1.0545	1.0354	0.9102	12.63/1.95/1.72	1.0184	1.1376	40	0.7514 ± 0.0172	1.2304 ± 0.0067	323.2 ± 10.0
TD248	9	1.0508	1.0074	0.9418	4.27/2.73/1.62	1.0432	1.0697	61	0.2179 ± 0.1356	1.1367 ± 0.0235	316.6 ± 10.5
Vichenet Formation (Wenlock), Vichenet section, Orneau valley											
TD1020	6	1.0607	0.9796	0.9597	3.95/16.07/3.18	1.0828	1.0207	74	−0.5909 ± 0.0694	1.1508 ± 0.0135	311.5 ± 7.9
TD1023	6	1.0581	0.9908	0.9511	4.85/9.70/3.25	1.0680	1.0418	60	−0.2336 ± 0.1343	1.1397 ± 0.0086	316.7 ± 6.6
TD1026	6	1.0547	1.0064	0.9389	9.58/7.05/4.08	1.0479	1.0719	46	0.1935 ± 0.0769	1.1430 ± 0.0118	240.8 ± 7.9
TD1025	5	1.0555	1.0012	0.9432	4.48/4.30/2.20	1.0543	1.0615	41	0.0614 ± 0.0501	1.1276 ± 0.0167	274.6 ± 16.2
TD1021	4	1.0589	0.9738	0.9673	1.40/19.05/1.33	1.0873	1.0068	87	−0.8515 ± 0.0356	1.1467 ± 0.0011	250.8 ± 3.9
TD1021L	3	1.0398	0.9958	0.9645	5.03/7.03/2.97	1.0442	1.0324	87	−0.1509 ± 0.0477	1.0921 ± 0.0036	295.3 ± 5.4
Ronquières Formation (Ludlow), Inclined Shiplift of Ronquières, Sennette valley											
TD1	8	1.0370	0.9848	0.9782	4.05/32.51/3.56	1.0531	1.0067	76	−0.7730 ± 0.0957	1.0897 ± 0.0090	315.4 ± 8.4
TD2	7	1.0380	0.9834	0.9786	2.70/30.39/2.44	1.0556	1.0048	87	−0.8379 ± 0.0758	1.0922 ± 0.0017	295.6 ± 7.2
TD3	6	1.0325	0.9879	0.9797	14.63/54.72/12.10	1.0452	1.0083	88	−0.7013 ± 0.1992	1.0781 ± 0.0118	311.8 ± 9.9
TD4	8	1.0346	0.9862	0.9791	12.89/40.76/11.50	1.0491	1.0073	86	−0.7264 ± 0.1160	1.0837 ± 0.0177	315.7 ± 7.6
TD5	8	1.0361	0.9879	0.9760	9.38/31.20/7.20	1.0488	1.0121	86	−0.5949 ± 0.1803	1.0868 ± 0.0072	307.7 ± 7.4
TD6	10	1.0363	0.9892	0.9745	4.26/13.76/3.26	1.0475	1.0150	90	−0.5152 ± 0.0663	1.0870 ± 0.0057	298.5 ± 6.4

Table 1. *(cont.)*

Sample	n	K1	K2	K3	95% confidence E12/E23/E13	Lineation L	Foliation F	Angle S0–S1	Shape parameter T	Degree of anisotropy Pj	Mean suscept.
Additional samples											
Asquempont Member, Oisquercq Formation (Lower to lower Middle Cambrian), Virginal Railway section, Sennette valley											
TD1031	6	1.0526	1.0033	0.9441	13.08/13.27/6.93	1.0492	1.0628	50	0.1186 ± 0.1319	1.1319 ± 0.0300	254.5 ± 5.6
TD1032	9	1.0482	1.0194	0.9324	7.30/2.42/1.81	1.0283	1.0933	30	0.5231 ± 0.0265	1.1672 ± 0.0067	311.8 ± 8.8
Neoproterozoic turbidites, Central Dobrogea, Moesian Platform, Romania											
TDD1	10	1.0338	1.0003	0.9659	4.17/4.43/2.11	1.0335	1.0357	88	0.0119 ± 0.1488	1.0773 ± 0.0167	361.8 ± 27.3
TDD3	8	1.0253	1.0134	0.9613	9.15/2.14/1.73	1.0118	1.0542	55	0.6367 ± 0.0169	1.0932 ± 0.0039	280.2 ± 4.5
TDD4	14	1.0298	1.0153	0.9549	8.71/2.08/1.69	1.0143	1.0633	22	0.6251 ± 0.0320	1.1094 ± 0.0043	367.0 ± 25.8
TDD5	6	1.0141	1.0002	0.9857	8.55/8.48/4.28	1.0139	1.0146	73	0.0208 ± 0.1062	1.0316 ± 0.0031	290.3 ± 10.8
TDD6	9	1.0298	1.0172	0.9530	14.84/2.94/2.44	1.0124	1.0673	27	0.6828 ± 0.0393	1.1144 ± 0.0057	333.5 ± 13.0

N: number of specimens; K1, K2, K3: mean maximum, intermediate and minimum principal susceptibility axis; E12, E23, E13: mean 95% confidence angles of K1, K2 and K3; lineation L = K1/K2; foliation F = K2/K3; angle S0–S1: angle between cleavage and bedding; shape parameter $T = (2\eta_2 - \eta_1 - \eta_3)/(\eta_1 - \eta_3)$, with $\eta_1 = \ln K1$, $\eta_2 = \ln K2$, and $\eta_3 = \ln K3$ (Jelínek 1981); corrected degree of anisotropy $Pj = \exp 2[(\eta_1 - \eta_m)^2 + (\eta_2 - \eta_m)^2 + (\eta_3 - \eta_m)^2]^{1/2}$, with $\eta_m = (\eta_1 \eta_2 \eta_3)^{1/3}$ (Jelínek 1981); mean susceptibility = (K1 + K2 + K3)/3, expressed in 10^{-6} SI. In the case of the shape parameter, the corrected degree of anisotropy and the mean susceptibility, standard deviations are added in order to give an idea about possible variations between different specimens of the same sample.

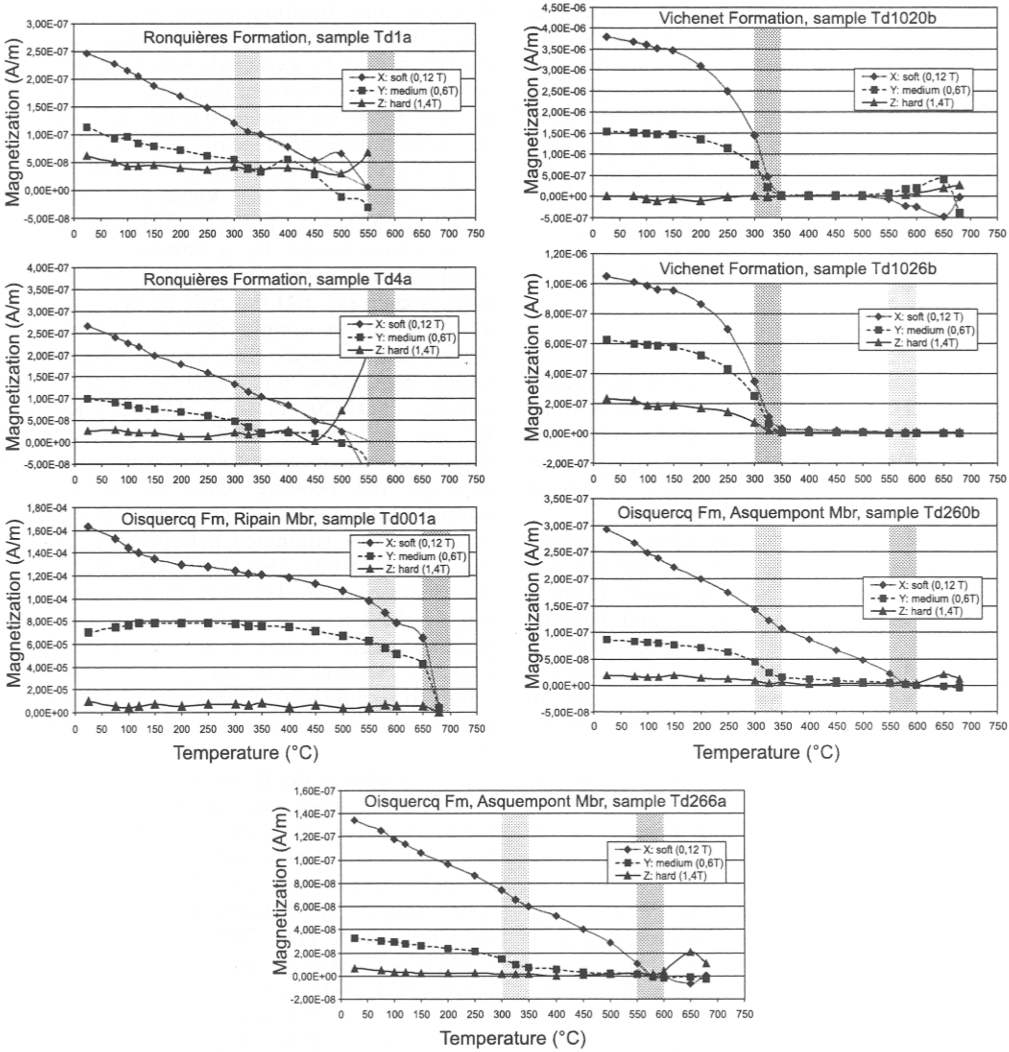

Fig. 3. Demagnetization curves of one sample of the Ripain Member (TD001), two samples of the Asquempont Member (TD260 and TD266), two samples of the Vichenet Formation (TD1020 and TD1026) and two samples of the Ronquières Formation (TD1 and TD4). The dark grey band shows the demagnetization temperature interval of the dominant ferromagnetic carrier (hematite in TD001, magnetite in TD260, TD266, TD1 and TD4, and pyrrhotite in TD1020 and TD1026), the pale grey band that of the additional ferromagnetic component (magnetite in TD001 and TD1026, pyrrhotite in TD260, TD266, TD1 and TD4). Note, that in sample TD001 (Ripain Member) the presence of hematite is reflected by the soft and medium component curves, and not, as one would expect, by the hard component curve. Probably this reflects low-coercivity, multidomain hematite (cf. Robion *et al.* 1997).

of 670 °C), with, however, a medium to low coercivity (>0.6 T). Such low-coercivity hematite was already observed in upper Lochkovian slates on the Rocroi massif in the Ardennes (Robion *et al.* 1997) and was attributed to the presence of coarse-grained hematite. Magnetite and possibly some goethite are also observed in these samples but only in small amounts. The Asquempont Member of the Oisquercq Formation, in contrast, has a ferromagnetic mineralogy dominated by magnetite (blocking temperature around 580 °C and low coercivity), with a small amount of pyrrhotite (blocking temperature between 325 and 350 °C and medium coercivity). The ferromagnetic mineralogy of the Vichenet Formation is dominated by pyrrhotite. This pyrrhotite shows a wide range of coercivities, but mainly controls the low coercivity component. One of the two analysed samples of this lithology shows a small amount of additional magnetite (TD1026). The sampled bed within the Ronquières Formation has a ferromagnetic mineralogy entirely consisting of magnetite, with locally a minor amount of pyrrhotite (Fig. 3).

Anisotropy of magnetic susceptibility

Orientation analysis

In all analysed samples the maximum susceptibility axis (K1) coincides with the cleavage/bedding intersection (Fig. 4). However, in the case of the minimum susceptibility axis (K3), strong variations may occur, seemingly unrelated to lithology or structural position.

In samples of the Ripain Member, all characterized by a small angle between cleavage and bedding (maximum 26°), K3 generally forms a cluster in between the cleavage and bedding poles (Fig. 4). In some samples, K3 tends to approximate the bedding pole (e.g. TD001, TD1002), whereas in other samples it tends to approximate the cleavage pole (e.g. TD002, TD256, TD1001). Although in all samples a rather small angle occurs between cleavage and bedding, we do not think that this deviation from the cleavage or bedding pole is due to errors induced by orientation and cutting irregularities.

In samples of the Asquempont Member, K3 generally clusters around the bedding pole (Fig. 4; samples TD274, TD266, TD248, TD003, TD271, TD260, TD197, TD1003). Seemingly, two exceptions occur. In sample TD262, the position of K3 in between the bedding and cleavage poles may be an artefact due to the small angle between cleavage and bedding, in combination with orientation or cutting irregularities. For TD1004, the position of K3, closer to the cleavage pole than to the bedding pole, may also be an artefact. Unlike in the case of cubes, cut from oriented hand specimens on which bedding and cleavage orientation were determined, in the case of cylinders (TD1004, TD1003) cleavage and bedding orientation were not taken from the cylinder itself. Hence, a small mismatch may be expected, which, in the case of a small angle between cleavage and bedding, will not allow determining whether K3 approximates the pole to cleavage or the pole to bedding or takes up a truly intermediate position.

The samples of the Vichenet Formation (TD1021, TD1020, TD1025, TD1026) appear to be characterized by a sub-horizontal K3, occupying an intermediate position between the pole to cleavage and the pole to bedding (Fig. 4). Although in sample TD1021, K2 and K3 show a marked girdle distribution, reflecting its strong prolateness (cf. Table 1), in the other samples (TD1020, TD1025, TD1026) K2 and K3 are well defined, reflecting truly triaxial ellipsoids with an orientation in between that of cleavage and bedding. Only in the case of sample TD1023 does K3 coincide with the pole to cleavage. A laminated hemipelagite, present in sample TD1021, also shows a K3 parallel to the cleavage pole. The fact that in the same sample the e-interval, with the same cleavage/bedding angle, shows a K3 in between the pole to cleavage and the pole to bedding, points to an influence of lithology on the orientation of the minimum axis of the susceptibility ellipsoid.

The samples of the Ronquières Formation, all taken from a single bed across the central antiform (e-interval of turbidite sequence 121 of Verniers *et al.* 1992), are characterized by a strongly variable K3 orientation (Fig. 4). In some samples K3 clusters around the pole to cleavage (TD2, TD4, TD6), whereas in other samples K3 takes up an intermediate position (TD3, TD5, TD1), in some cases closer to the bedding pole (TD1), in other cases closer to the cleavage pole (TD5). These variable relative orientations do not appear to show any relationship with the position within the fold (cf. Fig. 2). Many samples have K2-K3-girdles, reflecting a strong prolateness (e.g. TD1, TD3, TD4; cf. table 1), and hence a rather poorly defined nature of K3. However, the confidence ellipses suggest that the mismatches between K3 and the poles to the macroscopic fabric elements are significant.

Fig. 4. Lower-hemisphere equal-area stereographic projections showing the principal magnetic susceptibility axes (K1, K2, K3; K1 > K2 > K3), the 95% confidence ellipses for the principal magnetic susceptibility axes, bedding (pole and plane) and cleavage (pole and plane) of samples of the Ripain Member (outcrop Northern Asquempont section), the Asquempont Member (outcrop Northern Asquempont section), the Vichenet Formation (outcrop Vichenet section) and the Ronquières Formation (central antiform in outcrop Ronquières section; Inclined shiplift of Ronquières). Samples are shown going from N to S along each outcrop. See Fig. 2 for sample location. LHP: laminated hemipelagite (sample TD1021, Vichenet Formation).

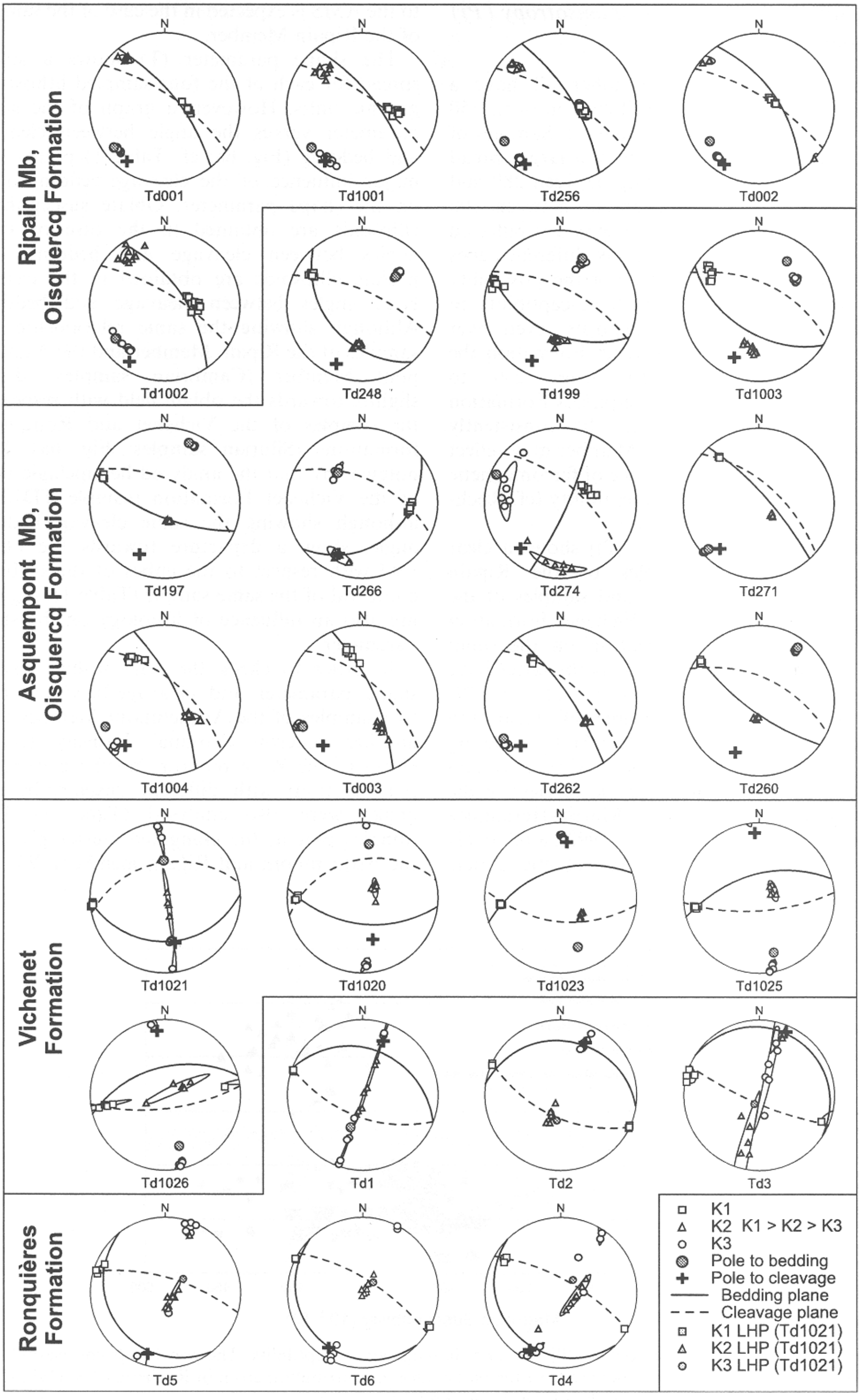
Ripain Mb, Oisquercq Formation
Td001
Td1001
Td256
Td002
Td1002
Td248
Td199
Td1003
Asquempont Mb, Oisquercq Formation
Td197
Td266
Td274
Td271
Td1004
Td003
Td262
Td260
Vichenet Formation
Td1021
Td1020
Td1023
Td1025
Td1026
Td1
Td2
Td3
Ronquières Formation
Td5
Td6
Td4
K1
K2 K1 > K2 > K3
K3
Pole to bedding
Pole to cleavage
Bedding plane
Cleavage plane
K1 LHP (Td1021)
K2 LHP (Td1021)
K3 LHP (Td1021)

Bulk susceptibility, degree of anisotropy (Pj) and shape parameter (T)

Samples of the Ripain Member all have a relatively high bulk susceptibility between 350 and 460×10^{-6} SI (Fig. 5, Table 1). Samples of the Asquempont Member show a large spread in bulk susceptibility, ranging between 280 and 470×10^{-6} SI, with a maximum between 300 and 400×10^{-6} SI. This large spread is reflected both by different samples as by different cubes of the same samples, indicating the possibility of a strong variation in bulk susceptibility in apparently homogeneous deposits, even over short distances. In the Vichenet Formation the bulk susceptibility ranges from 230 to 330×10^{-6} SI and in the Ronquières Formation from 280 to 330×10^{-6} SI. The consistently higher values of the Ripain Member may reflect a relatively important influence of ferromagnetic carriers to the magnetic susceptibility (cf. Rochette *et al.* 1992; Hrouda 2002).

The degree of anisotropy (Pj) shows a clear difference between samples of the Ripain Member on the one hand, and samples of the Asquempont Member, the Vichenet Formation and the Ronquières Formation on the other hand (Fig. 5, Table 1). Whereas the latter have a degree of anisotropy between 1.02 and 1.21, the former all have a degree of anisotropy higher than 1.29, ranging up to 1.51. Considering that the degree of anisotropy of white mica and chlorite, the main paramagnetic carriers in the investigated samples, is 1.15 (Martín-Hernández & Hirt 2003; cf. Rochette *et al.* 1992), a relatively important contribution of ferromagnetic carriers to the AMS is expected in the case of the samples of the Ripain Member.

The shape parameter (T) shows a strong spread for each of the four sampled lithostratigraphic units. However, a graph of the shape parameter versus the angle between cleavage and bedding (Fig. 6a; cf. Table 1) points to a major influence of the cleavage/bedding angle on the shape parameter. Oblate susceptibility ellipsoids are obtained in the case of small angles between cleavage and bedding, and prolate ellipsoids are obtained in the case of large angles between cleavage and bedding. Although showing the same relationship, the samples of the Ripain Member and the Asquempont Member (Cambrian samples) depart slightly towards the oblate field with respect to the samples of the Vichenet and Ronquières formations (Silurian samples; Fig. 6a). It is noteworthy that the analysed hemipelagic parts of the Vichenet Formation (sample TD1021), although showing the same cleavage/bedding angle, show a departure towards the oblate field with respect to the cubes of the turbidite e-interval of the same sample (Table 1), suggesting also an influence of lithology on the shape parameter.

In order to check the relationship between shape parameter and cleavage/bedding angle, two samples of the Asquempont Member from another outcrop (Virginal Railway section, 600 m to the W of outcrop Northern Asquempont section) with different cleavage/bedding angles were also analysed (Table 1). Both samples plot in the elongated cluster given by the Asquempont and Ripain members. We also

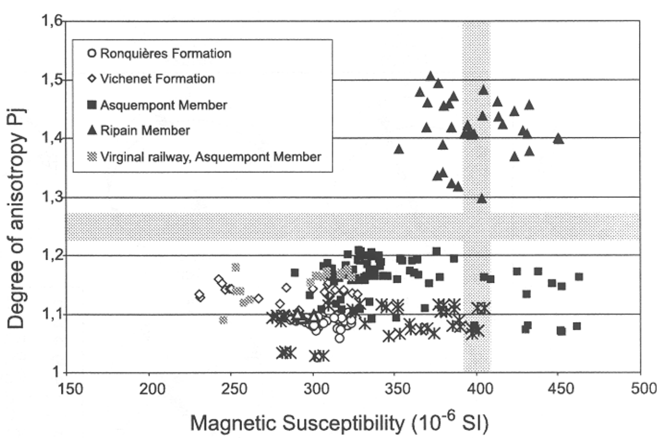

Fig. 5. Graph of degree of anisotropy (Pj) versus bulk magnetic susceptibility. The grey bands correspond to the mean of the approximate upper limits of the paramagnetic contribution given in Rochette *et al.* (1992). Note the high Pj-values of the samples of the Ripain Member.

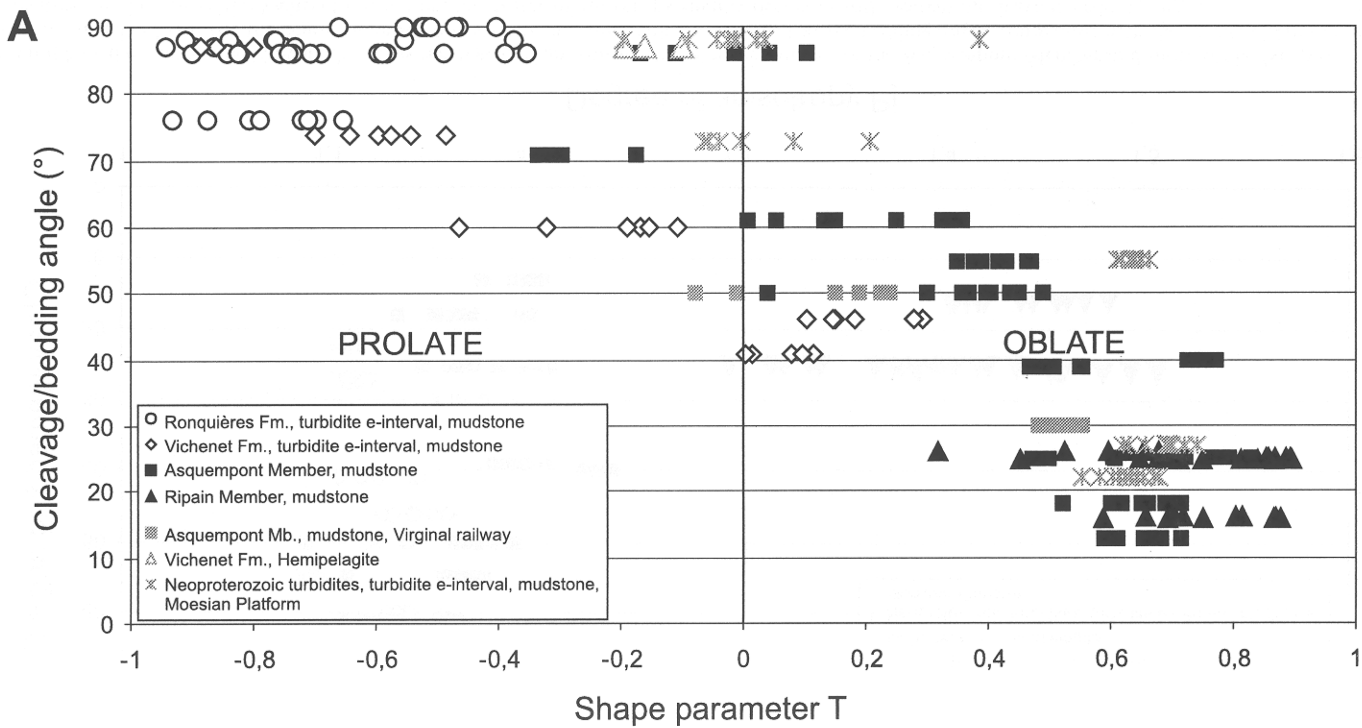

Fig. 6. (**a**) Graph of cleavage/bedding angle versus shape parameter (T). A marked relationship becomes apparent: low angles give rise to oblate susceptibility ellipsoids whereas high angles give rise to prolate ellipsoids. Note that the samples of the Vichenet and Ronquières formations (Silurian samples) show a slight shift towards the prolate field with respect to the samples of the Ripain and Asquempont members (Cambrian samples). In addition, note the marked difference in shape parameter between the e-interval and a laminated hemipelagite of the same sample (TD1021) of the Vichenet Formation.

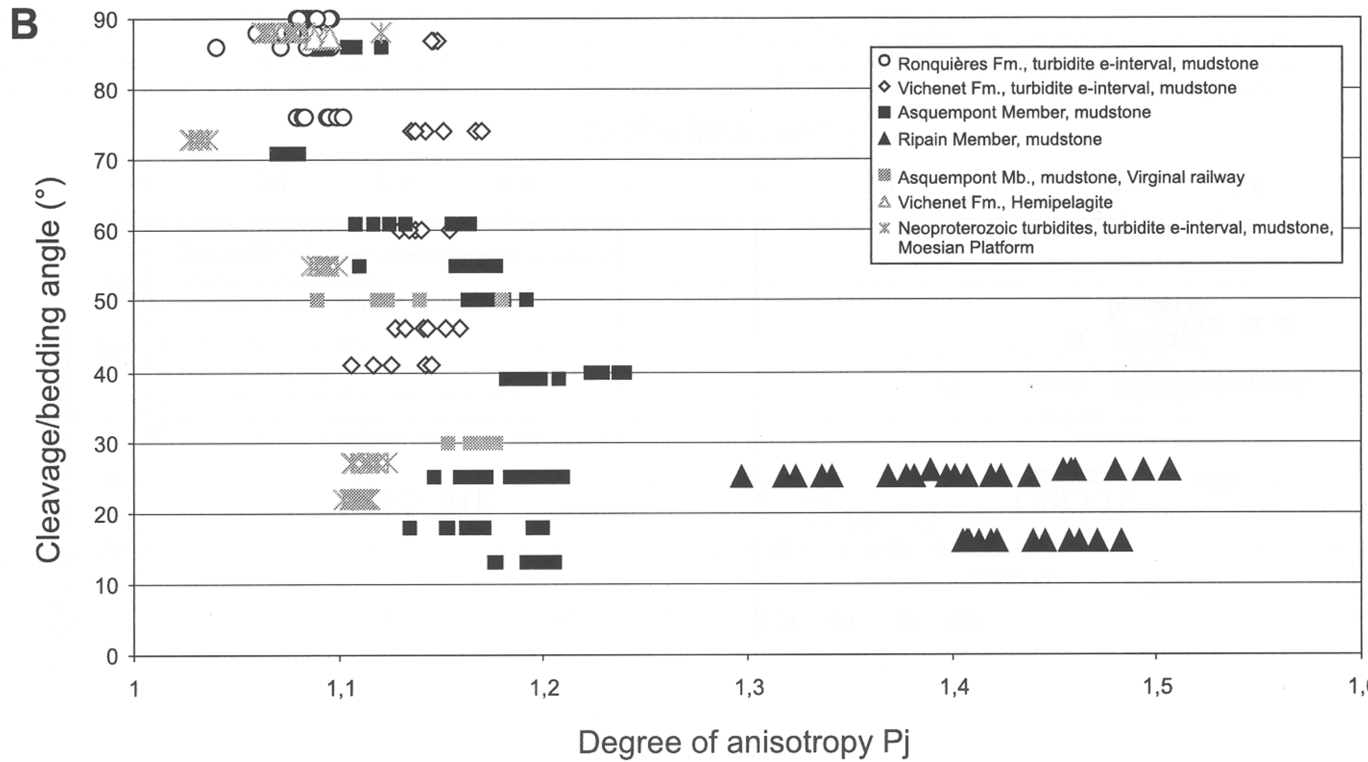

Fig. 6. (**b**) Graph of the cleavage/bedding angle versus the degree of anisotropy (Pj). For the samples of the Asquempont Member and those of the Neoproterozoic turbidites of the Moesian Platform, the degree of anisotropy slightly increases with decreasing cleavage/bedding angle, compatible with the results of Housen *et al.* (1993). In contrast, in the case of the Vichenet Formation, the degree of anisotropy slightly decreases with decreasing cleavage/bedding angle.

included five samples with different cleavage/bedding angles from fine-grained e-intervals of Neoproterozoic turbidites from five different outcrops of the Moesian Platform, Central Dobrogea (Romania; Table 1). Again, a similar relationship becomes apparent between the shape parameter and the cleavage/bedding angle (Fig. 6a). The one sample showing a slight departure towards the oblate field, macroscopically has a cleavage that is better developed than in the other samples. The fact that this relationship between T and the cleavage/bedding angle is also reflected by the samples of the Moesian platform indicates that it is not a regional phenomenon.

A graph of the degree of anisotropy Pj versus the cleavage/bedding angle shows that this angle also has an influence on the degree of anisotropy (Fig. 6b). However, this influence is different for the samples of the Vichenet Formation on the one hand and the samples of the Asquempont and Ripain members and those of the Moesian platform on the other hand (Fig. 6b; cf. Fig. 7). In the former case, the degree of anisotropy decreases slightly with decreasing cleavage/bedding angle, whereas in the latter case, the degree of anisotropy increases with decreasing cleavage/bedding angle.

Anisotropy of anhysteretic remanent magnetization (AARM)

Orientation of principal axes with respect to macroscopic fabric elements and AMS axes

Seemingly, the axes of AARM are more difficult to link to the macroscopic fabric elements (bedding, cleavage) than the axes of the magnetic susceptibility ellipsoids. Whereas in the latter case, K1 always coincides with the cleavage/bedding intersection and only K3 shows a variation with respect to the macroscopic fabric elements, in the case of the anhysteretic remanence, both the maximum axis (R1) and the minimum axis (R3) have variable orientations with respect to the macroscopic fabric elements (Fig. 8, Fig. 10).

In all analysed samples of the Oisquercq Formation (Ripain Member and Asquempont Member), R3 consistently clusters around the bedding pole, showing a large spread in the case of the Asquempont Member, whereas R1 takes up a position within to possibly slightly oblique to the bedding plane, at high, but variable angles to the cleavage/bedding intersection (Fig. 8). The high-angle obliquity between R1 and the cleavage/bedding intersection, occurring in three samples, all having completely different cleavage/bedding relationships, indicates that R1 is likely to mark a pre-deformational feature, which is compatible with R3 approximately coinciding with the bedding pole. For this reason, in each of the investigated samples bedding was unfolded to horizontal, using the local cleavage/bedding intersection as an approximation of the local fold axis. After unfolding, each of the samples, both from the Ripain Member and the Asquempont Member, shows a sub-horizontal to gently N- to NNE-plunging R1 (Fig. 8). This ferromagnetic lineation, probably caused by coarse-grained hematite in the case of the Ripain Member and by magnetite in the case of the Asquempont Member, is oriented sub-perpendicular to sedimentary ripples recorded in deposits of the Asquempont Member.

Because of the presence of two populations of ferromagnetic carriers in the samples of the Ripain Member, as indicated by the coercivity spectra (Fig. 9), pAARM was performed for the field between 0 and 50 mT (low coercivity window) and for the field between 50 and 100 mT (high coercivity window) (Fig. 8). The low-coercivity R3, thought to be caused by the preferred orientation of larger ferromagnetic grains (cf. Jackson *et al.* 1988), clusters around the bedding pole, whereas those of the high coercivity window, probably caused by smaller ferromagnetic grains (cf. Jackson *et al.* 1988), take up a position in between the bedding pole and the cleavage pole (Fig. 8). Although this is a very small angular difference, of which the significance might be questioned considering the accuracy of the JR5 spinner magnetometer, this difference is consistent for all analysed samples. Possibly, this difference reflects a partial rotation of the smaller ferromagnetic grains away from the bedding towards the cleavage, and hence a tectonic influence on the high-coercivity fraction, which seemingly is not reflected by the ferromagnetic fraction with a larger grain-size. This is also reflected by the R1 of one of the samples (Fig. 8): whereas R1 is oriented somewhere in the bedding plane, at high angles to the cleavage/bedding intersection in the case of AARM and low-coercivity pAARM, R1 of the high-coercivity pAARM has an orientation sub-parallel to the cleavage/bedding intersection, thus reflecting some tectonic influence on the smaller ferromagnetic grains in one of the samples.

In the Vichenet Formation, the results differ from sample to sample (Fig. 10). In sample TD1020, R3 of AARM, low-coercivity pAARM and high-coercivity pAARM all cluster

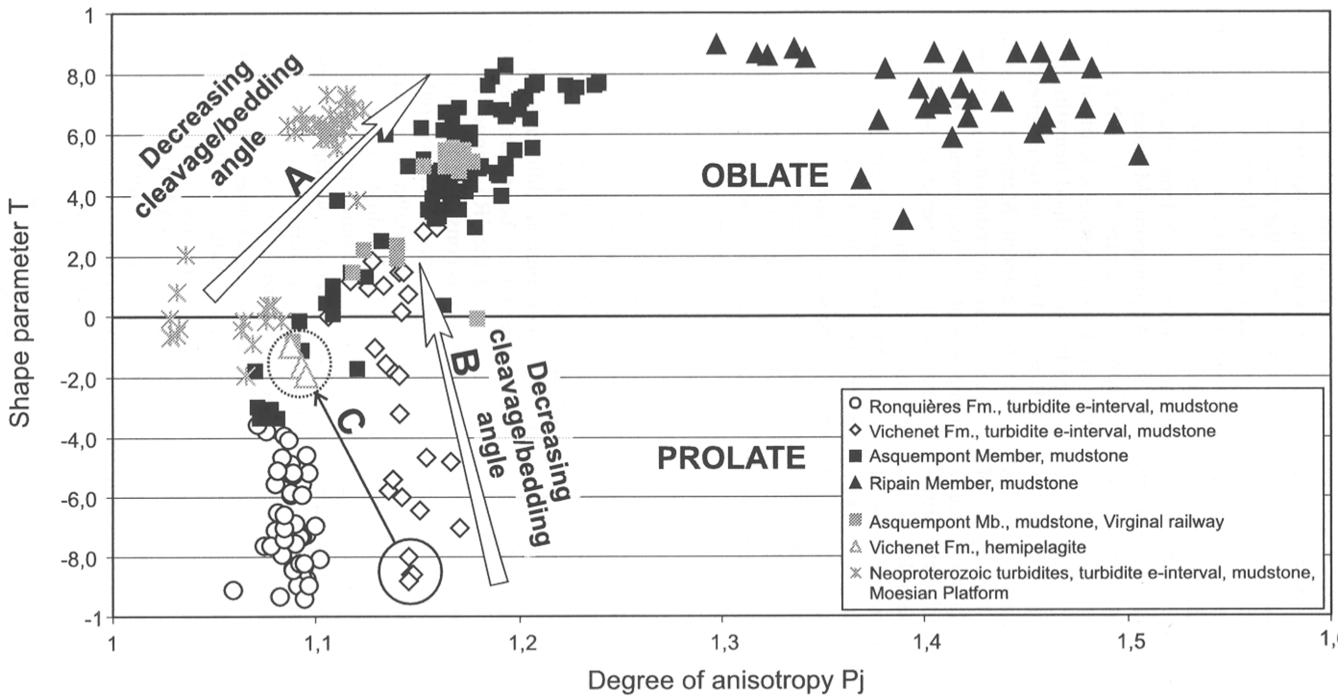

Fig. 7. Graph of the shape parameter (T) versus the degree of anisotropy (Pj). The isolated position of the Ripain Member is due to the small angle between cleavage and bedding (resulting in high T; cf. Fig. 6a) and to a relatively important contribution of ferromagnetic carriers (resulting in a relatively high Pj). Two trends can be observed in the other samples, both coinciding with a decrease in angle between cleavage and bedding. In samples of the Asquempont Member and of the Neoproterozoic turbidites, a decrease in cleavage/bedding angle results in an increase in T (cf. Fig. 6a) and a slight increase in Pj (arrow A; cf. Fig. 6b). In contrast, in samples of the Vichenet Formation, a decrease in cleavage/bedding angle also results in an increase in T (cf. Fig. 6a) but is accompanied by a slight decrease in Pj (arrow B; cf. Fig. 6b). Note that, although the cleavage/bedding angle remains the same, as well as the mean grain size, a small change in lithology/sedimentology (turbidite e-interval on the one hand versus laminated hemipelagite on the other hand) can cause large differences in Pj and T, as demonstrated by sample TD1021 of the Vichenet Formation (arrow C).

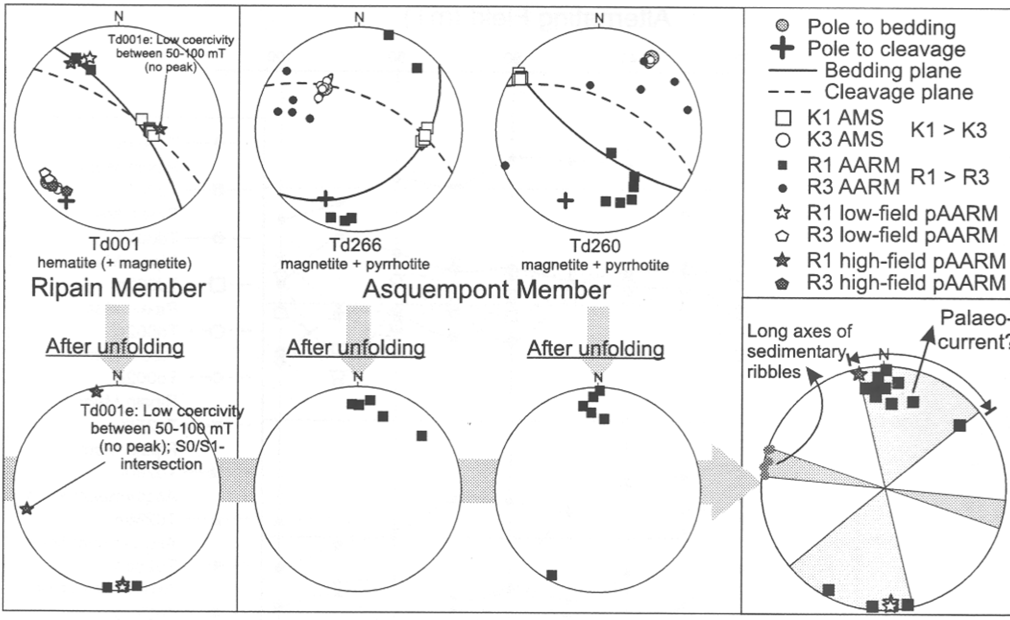

Fig. 8. Lower-hemisphere equal-area stereographic projections showing the principal axes of anisotropy of anhysteretic remanent magnetism (AARM), partial AARM (pAARM), AMS and macroscopic fabric element data of selected samples of the Oisquercq Formation. Unfolding the data around the local cleavage/bedding intersection (as an approximation of the local fold axis) gives similar orientations of the long axes of remanence for all samples, sub-perpendicular to sedimentary ribbles. See text for discussion.

around the cleavage pole, reflecting a tectonic control (cleavage-parallel) on the ferromagnetic carriers (pyrrhotite; cf. Fig. 3). The maximum axis of AARM and high-coercivity pAARM (small grains; cf. Jackson *et al.* 1988) coincides with the cleavage/bedding intersection, but R1 of low-coercivity pAARM, also situated within the cleavage plane, is markedly oblique to the cleavage/bedding intersection. Seemingly, this suggests that, although the majority of the ferromagnetic carriers, together with the small carriers, are tectonically controlled, but still influenced by the bedding fabric, the larger ferromagnetic carriers are not influenced by the original bedding fabric and hence fully controlled by the tectonic fabric. In sample TD1026, R1 of AARM and low-coercivity pAARM is steeply plunging within, or slightly oblique to the bedding plane, at high angles to the cleavage/bedding intersection, except for cube TD1026c, in which R1 of AARM plunges steeply within the cleavage plane. The minimum axis of AARM and low-coercivity pAARM is slightly oblique to the bedding pole, except for cube TD1026c that has an R3 of AARM that approaches the cleavage pole. In sample TD1025, the R3 of low-coercivity and high-coercivity pAARM coincides with the cleavage pole, whereas R1 of low-coercivity and high-coercivity pAARM is steeply plunging within the cleavage plane. This suggests a tectonic control on both the small and large ferromagnetic carriers, without there being an influence of the original bedding fabric.

Although taken from a single bed, the samples of the Ronquières Formation also give results that differ from sample to sample (Fig. 10). As in the case of AMS, the orientation of the minimum axis of AARM varies from sample to sample and does not always coincide with the pole to the macroscopic fabric elements. Because the coercivity spectra are all characterized by a single pronounced peak in the lower part of the spectrum, reflecting the presence of only one population (relatively large grains; Fig. 9; cf. Jackson *et al.* 1988), only the low-coercivity pAARM was determined. In sample TD1, R1 is situated within the bedding plane, oblique to the cleavage/bedding intersection, whereas R3 occupies a position in between the bedding pole and the cleavage pole, slightly closer to the latter. Possibly, this reflects a faint tectonic influence on the low-coercivity pAARM. In sample TD4, R1 coincides with the cleavage/bedding intersection, and R3 approximates the cleavage pole (and K3 of AMS), thus suggesting a tectonic

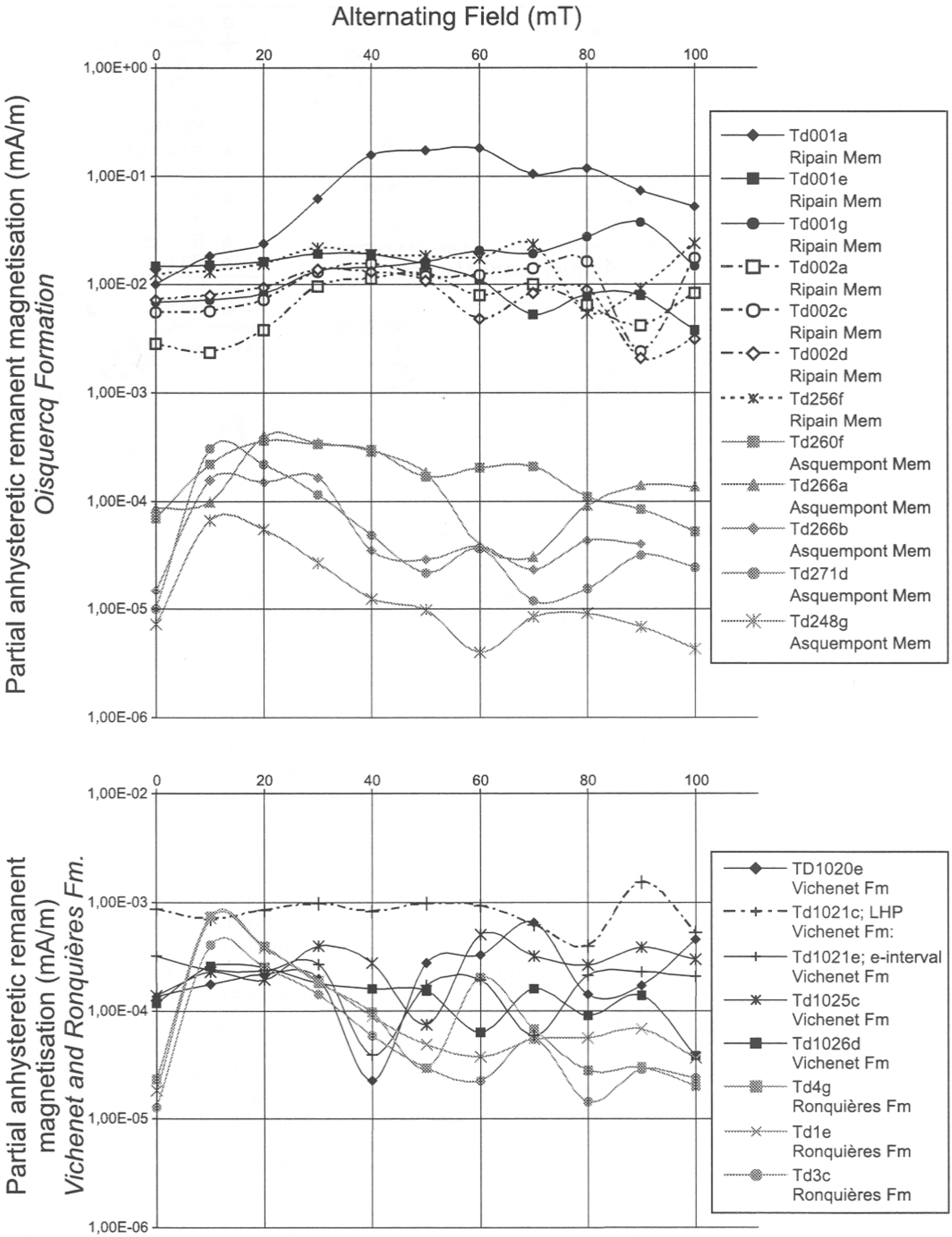

Fig. 9. Coercivity spectra of the Oisquercq Formation (above: Ripain and Asquempont members), the Ronquières Formation and the Vichenet Formation (below). In the latter case, also a laminated hemipelagite (LHP, cube TD1021c) has been analysed, adjacent to a turbidite e-interval (cube TD1021e) of the same sample (TD1021). Note the marked difference in remanent magnetization between the Ripain Member on the one hand and the Asquempont Member, the Vichenet Formation and the Ronquières Formation on the other hand. In addition, note the variation in remanent magnetization between different samples of the same lithology and even between different specimens of the same samples.

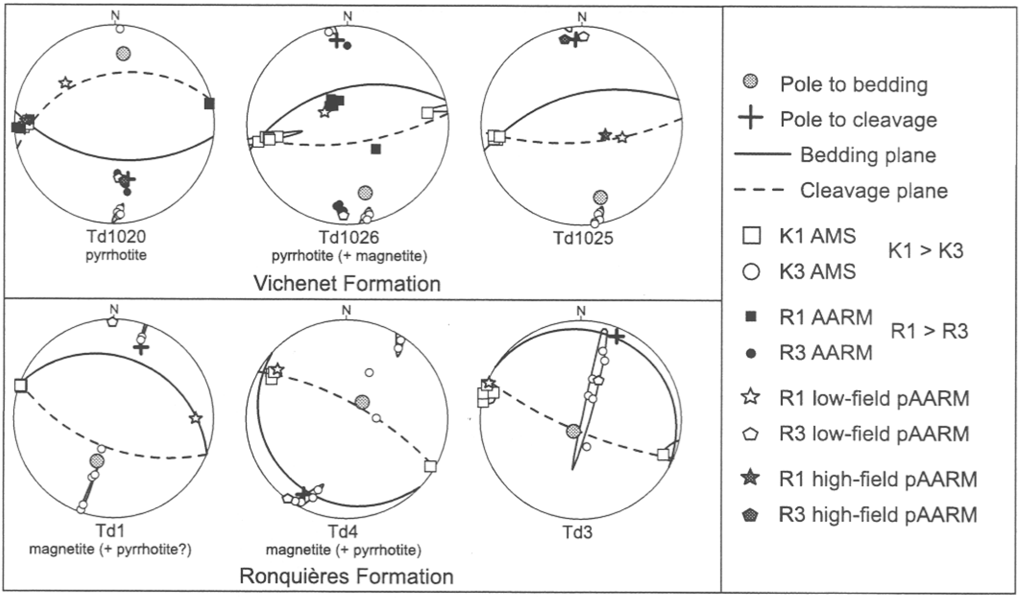

Fig. 10. Lower-hemisphere equal-area stereographic projections showing the principal axes of anisotropy of anhysteretic remanent magnetism (AARM), partial AARM (pAARM), AMS (cf. Fig. 4) and macroscopic fabric element data of selected samples of the Vichenet Formation and the Ronquières Formation. See text for discussion.

control on the orientation of the ferromagnetic carriers. In sample TD3, R1 coincides with the cleavage/bedding intersection, whereas R3 takes up an intermediate position in between the bedding pole and the cleavage pole, situated within the girdle-shaped cluster of K3 axes.

The above results show that often the axes of remanebility do not coincide with the axes of susceptibility. Together with the relatively low degrees of anisotropy and bulk susceptibility within the Ronquières Formation, the Vichenet Formation and the Asquempont Member, this suggests only a minor contribution of the ferromagnetic carriers to the AMS in these lithologies (cf. Hrouda & Jelínek 1990; Rochette *et al.* 1992; Hrouda 2002; Martín-Hernández & Hirt 2003). Only in the Oisquercq Formation does a consistent relationship appear to exist between the remanebility ellipsoid on the one hand and the susceptibility ellipsoid and the macroscopic fabrics on the other hand. In the case of the Ripain Member this is compatible with the relatively high degree of anisotropy and mean susceptibility, suggesting a relatively important contribution of the ferromagnetic fraction (cf. Hrouda & Jelínek 1990; Rochette *et al.* 1992; Hrouda 2002; Martín-Hernández & Hirt 2003).

Degree of anisotropy and shape parameter

The degree of anisotropy of AARM, Pj_R, shows a very large spread (Fig. 11). For nearly all samples, Pj_R is significantly higher than Pj (AMS), which, judging from the literature, is generally the case (Stephenson *et al.* 1986; Jackson 1991; Hrouda 2002). Only samples TD4g (Ronquières), TD260 and two cubes (c and d) of sample TD266 have nearly the same degree of anisotropy for AMS and AARM.

The shape parameter of AARM, T_R, shows a very strong variation, pointing to strongly prolate to strongly oblate AARM ellipsoids for the samples of the Ripain and Asquempont members, oblate to strongly oblate AARM ellipsoids for the Vichenet Formation, and 'plane strain' to strongly oblate AARM ellipsoids for the Ronquières Formation (Fig. 12). A comparison between T_R and T shows that there is no relationship between them. This suggests that the ferromagnetic mineralogy exerts only a minor influence on the shape of the AMS-ellipsoid. However, from this graph, a division becomes apparent between the Cambrian samples (Ripain and Asquempont members) and the Silurian samples (Vichenet and Ronquières formations). Whereas the former range from the

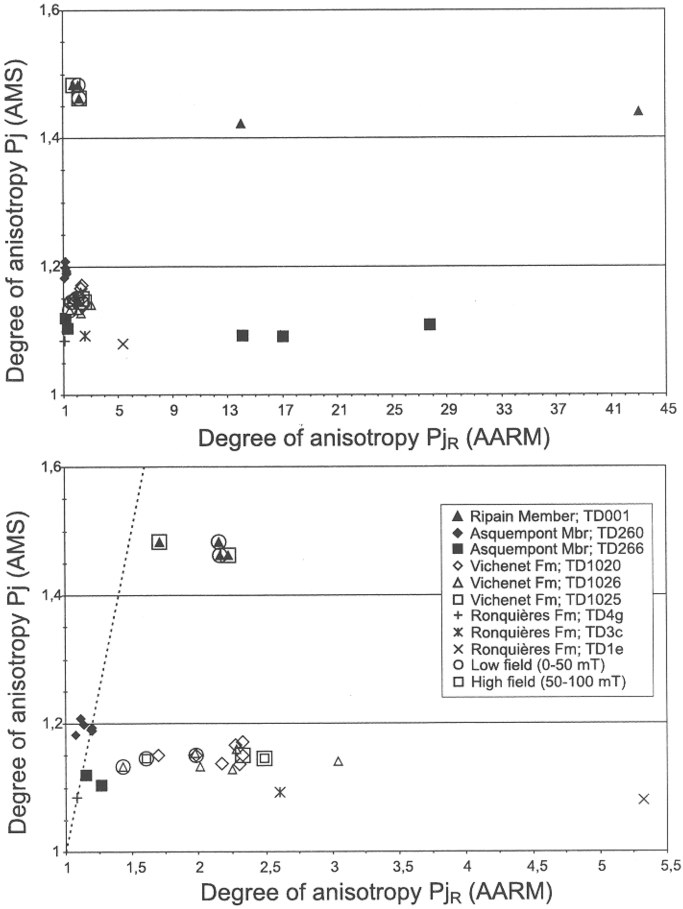

Fig. 11. Graphs of the degree of anisotropy of AMS (Pj) versus the degree of anisotropy of (p)AARM (Pj_R). The two graphs show the same data set, but with a different horizontal scale (Pj_R-scale). The stippled line in the lower graph represents the line on which Pj equals Pj_R. Note that the majority of the samples has a Pj_R that is much higher than Pj.

diagonal line towards the prolate AARM – oblate AMS field (above the diagonal line), the latter range from the diagonal line towards the oblate AARM – prolate AMS field (below the diagonal line). This division results partly from the difference in AMS ellipsoids, being more prolate in the Silurian for similar cleavage/bedding angles (cf. Fig. 6a), but also partly from the difference in AARM ellipsoids, apparently being more commonly slightly more prolate in the Cambrian samples.

X-ray pole figure goniometry

Judging from the overall mineralogy of the sampled lithologies (see above), the main paramagnetic carriers present are white mica and chlorite (cf. Geerkens & Laduron 1996; Debacker *et al.* 1999; Debacker 2001). Hence, phyllosilicate X-ray pole figure goniometry can be used to characterize the preferred orientation of these two paramagnetic carriers.

In the Oisquercq Formation, two main types of pole figure patterns can be distinguished (Fig. 13). The first type, from samples of the Asquempont Member and the Ripain Member, is characterized by a moderate (samples TD279, TD256, TD197), occasionally weak (sample TD186) preferred orientation (Fig. 13), with the maxima of both white mica and chlorite coinciding with the cleavage pole. The pole figure patterns have an axially symmetrical (e.g. sample TD279) to slightly orthorhombic shape

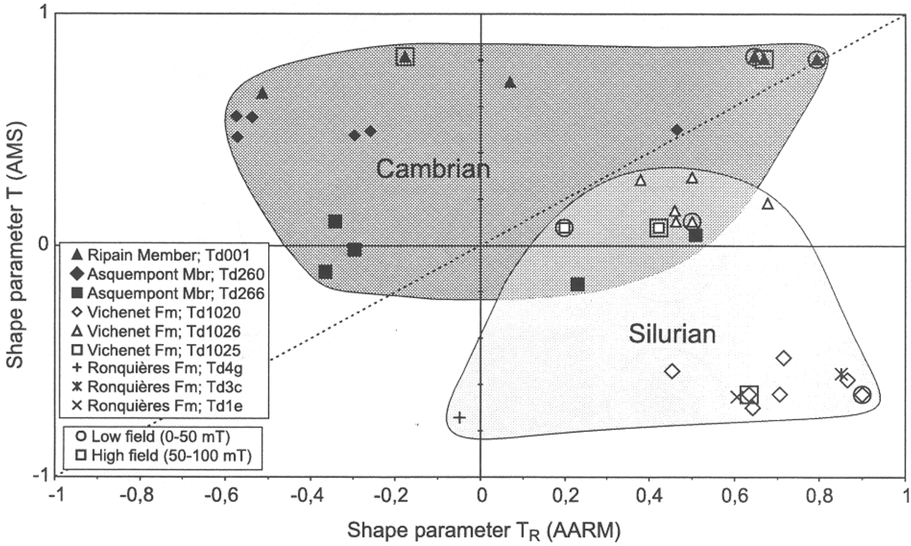

Fig. 12. Graph of the shape parameter of AMS (T) versus the shape parameter of (p)AARM (T_R). Although, from this graph, there appears to be no relationship between T and T_R, the Cambrian samples and Silurian samples occupy different fields. The stippled diagonal line represents the line of equal values.

(e.g. sample TD256). In the case of samples TD279 and TD179, the pole figure pattern reflects a flattening fabric. In contrast, the steeply plunging short axes of the slightly orthorhombic pole figure patterns of samples TD256 and TD186 may correspond to an intersection lineation between cleavage and bedding, which complies with the macroscopically observed steeply plunging cleavage/bedding intersection. The second and dominant type of pole figure, obtained from the Asquempont Member, both from zones of sub-horizontal and steeply plunging folds, has a clear girdle pole figure pattern, a relatively weak degree of preferred orientation, which is higher for chlorite than for white mica, and different pole figure maxima for chlorite and for mica (samples TD185, TD272, TD192, TD276, TD195, TD196 and TD248). The girdle pattern and the different pole figure maxima of chlorite and mica point to an intersection fabric. The mica pole figure maxima coincide with the cleavage pole, whereas the chlorite pole figure maxima approximate the bedding pole. This difference between mica and chlorite pole figure maxima, which, thus far, seems quite unique in the Brabant Massif (see Sintubin *et al.* 1998; Debacker *et al.* 1999; Belmans 2000; Piessens *et al.* 2000; Debacker 2001; Sintubin, unpublished data), is compatible with the macroscopically determined angle between bedding and cleavage (Fig. 13). Large differences between chlorite and mica pole figure maxima are obtained from samples with a large angle between bedding and cleavage (e.g. samples TD192, TD195, TD196), whereas small angles between chlorite and mica pole figure maxima are obtained from samples with a small angle between cleavage and bedding (e.g. sample TD272). In all samples, the short axis of the girdle corresponds to the cleavage/bedding intersection lineation.

The shape and the higher amount of preferred orientation of the first type of pole figure patterns as compared to the second type of pole figure patterns might be related to the rather small angle between bedding and cleavage. Indeed, there appears to be a relationship between the cleavage/bedding angle and the degree of phyllosilicate preferred orientation (Fig. 14).

As for the magnetic analyses, the samples for X-ray pole figure goniometry in the Ronquières section were taken from the e-interval of turbidite sequence 121 of Verniers *et al.* (1992; i.e. 30 to 65 cm below the lower, quartzitic, marker horizon depicted in Fig. 2). The results of this analysis have already been discussed in Debacker *et al.* (1999). There is no significant variation in degree of preferred orientation nor in pole figure pattern across the antiform. Both for mica and for chlorite an intersection pole figure pattern is apparent, reflecting the superposition of a cleavage fabric on a pre-existing,

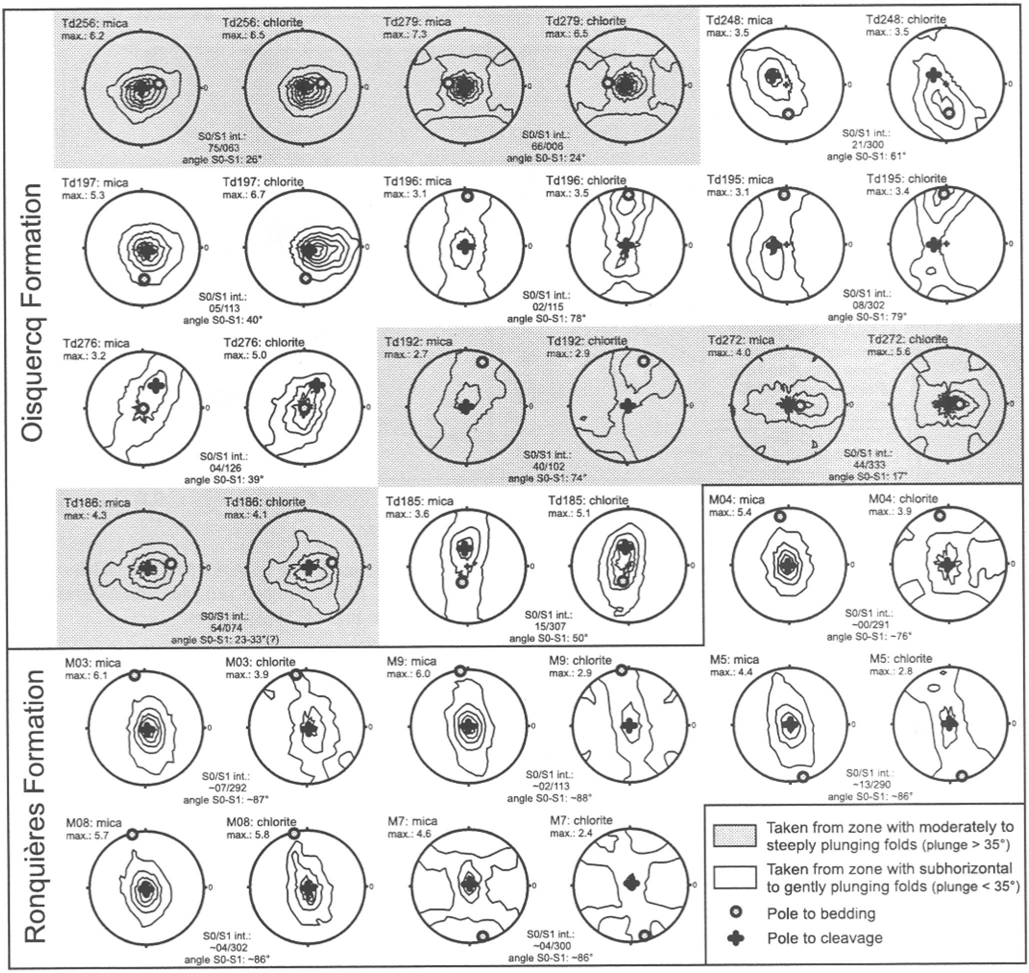

Fig. 13. Phyllosilicate X-ray pole figures of mica (d001; left) and chlorite (d002; right) from the Oisquercq Formation in the Northern Asquempont section (Cambrian) and the Ronquières Formation in the Ronquières section (Silurian; see Fig. 2 for sample location), together with the projected positions of the bedding and cleavage poles. Added are the orientation of the cleavage/bedding intersection, the angle between cleavage and bedding, and the maximum degree of preferred orientation, expressed in multiples of a random distribution (mrd). Note the occasional presence of axially symmetrical, flattening fabrics in the samples of the Oisquercq Formation and the overall predominance of orthorhombic to girdle patterns, reflecting intersection fabrics both in the Silurian and Cambrian samples. This intersection fabric is interpreted as resulting from a cleavage fabric (reflected by white mica) affecting a bedding-parallel compaction fabric (reflected by chlorite) (cf. Sintubin 1994*a*; Debacker *et al.* 1999). An important difference between the Cambrian samples and Silurian samples is that, whereas in the Silurian samples both the mica and chlorite maxima approximately coincide with the cleavage pole, in the Cambrian samples the intersection pole figure maximum approximately coincides with the bedding pole in the case of chlorite and with the cleavage pole in the case of mica.

bedding-parallel, compaction fabric (Fig. 13). The degree of preferred orientation of chlorite is weak. The chlorite pole figure pattern shows a clear girdle, with the cleavage/bedding intersection as symmetry axis. In contrast, mica shows a stronger degree of preferred orientation, with an orthorhombic pole figure pattern, centred around the cleavage pole. Also for mica, the short axis of the orientation distribution coincides with the cleavage/bedding intersection, implying that there are still remnants of a bedding-parallel compaction fabric, even

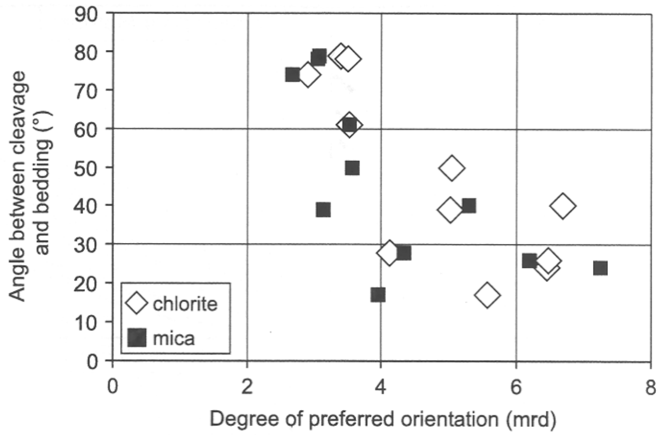

Fig. 14. Graph of the angle between cleavage and bedding versus degree of phyllosilicate preferred orientation, expressed in multiples of a random distribution (mrd) from samples of the Oisquercq Formation (outcrop Northern Asquempont section). Apparently, the degree of preferred orientation increases with decreasing cleavage/bedding angle. This happens both for mica and for chlorite.

though mica is preferentially oriented parallel to the cleavage.

Discussion

Comparison of AMS, AARM and X-ray pole figures: relative orientation and contribution of paramagnetic and ferromagnetic carriers to AMS

The coincidence of K1 with the cleavage/bedding intersection suggests an intersection fabric (Housen *et al.* 1993). Dealing with two fabric elements, a bedding fabric and a cleavage fabric, the mismatches between K3 (AMS) and the pole to one of these two fabric elements can be attributed to the presence of two or more different orientation populations of magnetic (*s.l.*) carriers (e.g. ferromagnetic carriers on the one hand and paramagnetic carriers on the other hand), of which some may be statistically oriented along the bedding, some along the cleavage, and possibly some oblique to both cleavage and bedding (e.g. due to an incomplete rotation away from the bedding plane towards the cleavage plane, or micro-kinking or bending of phyllosilicates). In the case of the Ripain Member, K3 is sometimes perpendicular to bedding, sometimes perpendicular to cleavage, and often takes up an intermediate position in between the bedding pole and the cleavage pole. The paramagnetic carriers, mica and chlorite, exhibiting a flattening fabric, appear to be situated statistically within the cleavage plane. In contrast, as indicated by (p)AARM, the ferromagnetic carriers (probably coarse-grained hematite) are situated within the bedding plane. Hence, the samples of the Ripain Member suggest a competition between cleavage-parallel paramagnetic carriers on the one hand and bedding-parallel ferromagnetic carriers on the other hand in controlling the orientation of the minimum AMS axis (Fig. 15). Indeed, the high degree of anisotropy (Pj) and the relatively high bulk susceptibility of the samples of the Ripain Member support a relatively strong influence of the ferromagnetic carriers on the AMS signal (cf. Rochette 1987*a*; Hrouda & Jelínek 1990; Hrouda 2002; Martín-Hernández & Hirt 2003). Possibly, the difference in relative position of K3 with respect to cleavage and bedding between the different samples results from small changes in relative concentration of ferromagnetic carriers (cf. Borradaile 1987). This idea is supported by the coercivity spectra, showing changes in coercivity of up to two orders of magnitude, both between different samples and between different cubes of the same samples (Fig. 9). However, in contrast to K3, K1 always coincides with the cleavage/bedding intersection. This probably results from the cleavage- and bedding-parallel nature of the paramagnetic, respectively ferromagnetic carriers. Because of the fabric-parallel alignment of both types of carriers, and the angle between them, they will both contribute to the cleavage/bedding intersection, without the relative concentration of ferromagnetic and paramagnetic carriers having a significant influence on the orientation of K1 (cf. Housen *et al.* 1993). However, although

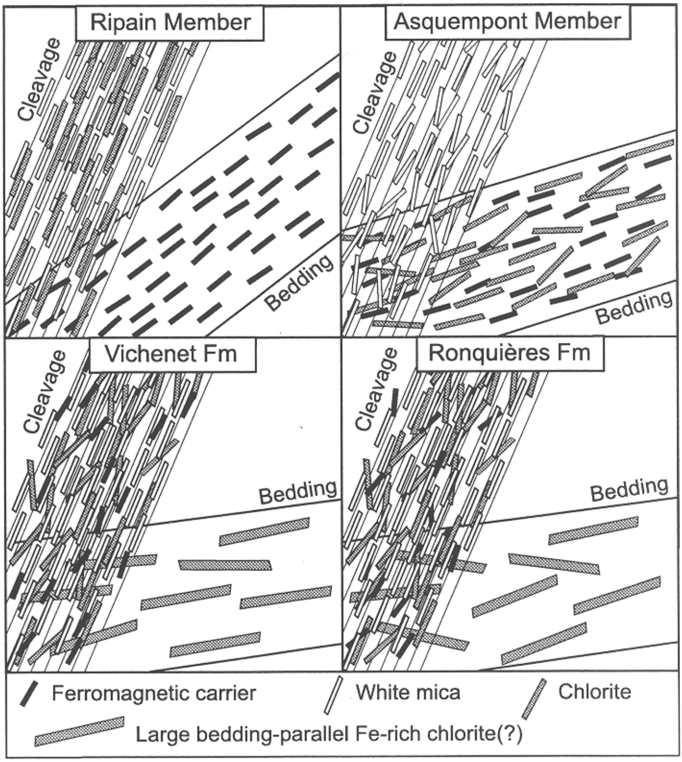

Fig. 15. Schematic representation of the probable magnetic (*s.l.*) fabric orientation with respect to bedding and cleavage in the Ripain Member of the Oisquercq Formation, the Asquempont Member of the Oisquercq Formation, the Vichenet Formation and the Ronquières Formation. The degree of alignment shown is based on X-ray pole figure goniometry data in the case of mica and chlorite and on the variation in orientation of R3 ((p)AARM) in the case of the ferromagnetic carriers. An important difference between the Cambrian samples (Ripain and Asquempont members of the Oisquercq Formation) and the Silurian samples (Vichenet and Ronquières formations) is the predominance of ferromagnetic carriers along the bedding in the former samples and along the cleavage in the latter samples. In order to explain the common mismatch between K3 and the pole to cleavage in the Silurian samples, we invoke the presence of paramagnetic carriers along the bedding plane. Likely candidates are large Fe-rich chlorites. Note that these bedding-parallel carriers are likely to be present also in the Cambrian samples. However, there, because of the relative orientations of the other carriers, their presence does not appear to affect the orientation of K3, and hence they are not depicted.

situated in the bedding plane, locally a slight tectonic influence on the ferromagnetic carriers is apparent, as suggested by R1 of high-coercivity pAARM of one of the cubes (TD001e). In this cube, the coincidence of R1 with the cleavage/bedding intersection, in combination with the position of R3 in between the cleavage pole and the bedding pole, indicates that the ferromagnetic carriers, probably with a relatively small grain-size (cf. Jackson *et al.* 1988), reflect an intersection fabric. This cube possibly also contains some additional ferromagnetic carriers that grew along the lattice of phyllosilicates (cleavage-parallel), thus reflecting an intersection fabric.

In the case of the Asquempont Member, K3 usually coincides with the bedding pole. Mica is statistically oriented along the cleavage plane, whereas chlorite is statistically oriented along the bedding plane. This implies that, even without the presence of ferromagnetic carriers, AMS would likely reflect an intersection fabric, with K1 parallel to the cleavage/bedding intersection and K3 either coinciding with the bedding pole, the cleavage pole, or taking up an intermediate position, all depending on the relative concentration and degree of preferred orientation of chlorite and mica. The ferromagnetic carriers are statistically situated within the bedding plane, thus accentuating the bedding-parallel AMS ellipsoid of chlorite. Hence, the position of K3 around the bedding pole may be attributed to the presence of both chlorite and ferromagnetic carriers along the bedding plane on the one hand and the presence of mica along the cleavage plane on the other hand (Fig. 15). Small shifts in K3 may be attributed to small changes in concentration and degree of preferred orientation of ferromagnetic carriers and chlorite on the one hand and mica on the other hand. Because of the angle between cleavage (mica) and bedding (chlorite and magnetite), all magnetic minerals (*s.l.*) contribute to the cleavage/bedding intersection, without the relative concentration of the carriers having a significant influence on the orientation of K1.

The orientation of R1 (AARM) within the Oisquercq Formation, having a high, but variable, angle with respect to the cleavage/bedding intersection suggests a pre-cleavage origin of the orientation reflected by the ferromagnetic carriers. Because after unfolding R1 has the same orientation in all samples, even in the presence of variable cleavage/bedding relationships (steeply plunging versus gently plunging folds), and always results in an orientation subperpendicular to sedimentary ripples, with a slight northward tilt within the bedding plane, we tentatively attribute R1 of the Oisquercq Formation to a preferred alignment due to palaeocurrents. Judging from the slight northward dip of the ellipsoids of remanence (plunge of R1) within the bedding plane, a southward palaeocurrent is inferred in the case of an imbrication of the ferromagnetic carriers. However, instead of showing an imbrication, the ferromagnetic minerals might also be oriented along low-angle foresets, in which case the inferred palaeocurrent would be towards the north.

In the Vichenet Formation, the majority of the samples has a sub-horizontal K3, situated in between the cleavage pole and the bedding pole. Unfortunately, we have no phyllosilicate X-ray pole figures of the Vichenet section. However, data from turbidite e-intervals 700 m to the north of the Vichenet section (the turbiditic, Wenlock Vissoul Formation of the Chenémont section; Belmans 2000; Sintubin, unpub. data) show the same pattern as the Ronquières Formation in the Ronquières section: mica and chlorite being statistically aligned along the cleavage plane, both exhibiting orthorhombic to girdle symmetries, with the cleavage/bedding intersection as symmetry axis and with a stronger degree of preferred orientation for mica. Hence, in order to explain the mismatch between K3 and the cleavage pole, one has to invoke the presence of a magnetic (*s.l.*) carrier sub-parallel to the bedding plane. However, in the three analysed samples, R3 usually coincides with the cleavage pole. This implies the presence of an unknown magnetic (*s.l.*) carrier parallel to bedding or with an orientation close to parallelism with bedding (Fig. 15), in order to explain the orientation of K3 in between the bedding pole and the cleavage pole. Judging from the relatively low bulk susceptibilities ($< 350 \times 10^{-6}$ Si) and the low degree of anisotropy, this is probably a paramagnetic carrier (Rochette 1987*a*; Hrouda & Jelínek 1990; Hrouda 2002). However, X-ray pole figure data suggest that the two main paramagnetic carriers, mica and chlorite, are likely to be oriented statistically parallel to cleavage. Still, optical microscopic observations show the presence of a significant number of chlorite-mica stacks parallel to bedding. Therefore, we suggest that, although chlorite is oriented statistically parallel to cleavage as suggested by X-ray pole figure goniometry, two different populations of chlorite may be present: small matrix chlorites, of a Mg-/Al-rich type, oriented parallel to cleavage, and larger, Fe-rich, chlorites, oriented parallel to bedding (e.g. chlorite/mica stacks). Whereas X-ray pole figure goniometry will preferentially show the preferred orientation of small, cleavage-parallel, matrix chlorites, AMS will be influenced mainly by the orientation of the relatively few Fe-rich chlorites, oriented parallel to bedding. As pointed out by several authors (e.g. Rochette *et al.* 1992; Borradaile & Werner 1994), the susceptibility of phyllosilicates is strongly controlled by their Fe-content. Hence, in combination with cleavage-parallel mica and ferromagnetic carriers, the presence of Fe-rich chlorites along the bedding plane should lead to a K3 situated in between the cleavage pole and the bedding pole. The coincidence of K1 with the cleavage/bedding intersection can be interpreted as the combined effect of the cleavage-parallel orientation of mica and ferromagnetic carriers on the one hand and the bedding-parallel orientation of Fe-rich chlorite on the other hand. In most samples, the maximum axis (R1) of (p)AARM, moderately to steeply plunging in the cleavage plane, at moderate to high angles to the cleavage/bedding intersection, points to a tectonic control on the ferromagnetic carriers. In sample TD1026, R1 reflects a predominantly bedding-parallel ferromagnetic carrier. This possibly represents a carrier that grew along the lattice of bedding-parallel chlorites.

In the Ronquières Formation, although taken from a single bed, the samples exhibit a strong variation in K3 orientation with respect to cleavage and bedding. In some cases, K3 coincides with the cleavage pole, whereas in other cases it takes up a position in between the cleavage pole and the bedding pole. X-ray pole figure goniometry indicates a preferred orientation of both mica and chlorite parallel to cleavage, with a higher degree of preferred orientation for mica, without showing a significant variation across the sampled antiform. Hence, considering the cleavage-parallel orientation of the phyllosilicates, the variation in K3 may be expected to be influenced by the variation in the orientation of the ellipsoid of remanence. Indeed, in some samples R3 is parallel to the pole to cleavage (e.g. TD4), whereas in other samples it occupies a position in between the cleavage pole and the bedding pole (e.g. TD3). In the cases where K3 parallels the pole to cleavage and R3 approximates the pole to cleavage, one may suggest a sub-parallelism of both the ferromagnetic and paramagnetic carriers within the cleavage plane. In contrast, however, considering that both mica and chlorite appear to be oriented along the cleavage plane, and that the ferromagnetic carriers do not appear to be situated within the bedding plane, it is difficult to explain the samples in which K3 takes up a position in between the pole to bedding and the pole to cleavage (e.g. TD1, TD3). In such cases, by analogy with the Vichenet Formation, we invoke the presence of a magnetic carrier along the bedding plane, of which the relative concentration may strongly affect the orientation of K3 (Fig. 15). We tentatively suggest Fe-rich bedding-parallel chlorite as a possible candidate. This Fe-rich chlorite may only have a minor influence on the X-ray pole figures (which predominantly reflect the finer-grained, omni-present matrix chlorites), but may dominate the AMS signal (cf. Rochette *et al.* 1992; Borradaile & Werner 1994). In all samples, R1 approaches the cleavage/bedding intersection. Together with the common proximity between the cleavage pole and R3, this suggests a slight tectonic control on the ferromagnetic carriers.

From the data and the above discussion, the complexity of the AMS fabric in the analysed samples becomes apparent, being influenced by both ferromagnetic and paramagnetic carriers. The isolation of the ferromagnetic signal does not always allow an explanation of all observations. In the case of the Silurian samples, the presence of a bedding-parallel, probably paramagnetic, carrier is proposed, in order to explain the observed AMS fabric. As a possible candidate we tentatively suggest large Fe-rich chlorites, which, because of their small numbers, are not detected by X-ray pole figure goniometry. Such a difference in preferred orientation of Fe-rich phyllosilicates and Fe-poor phyllosilicates was observed by Ho *et al.* (1995). However, in their example, the phyllosilicates oriented parallel to cleavage have a high iron content and those oriented parallel to bedding have a low iron content, whereas we suggest the reverse.

Influence of the cleavage/bedding angle

By means of experiments and numerical models, Housen *et al.* (1993) pointed out the influence of both the angle between two magnetic fabrics and the relative concentration of magnetic minerals along these fabrics on the shape parameter and the degree of anisotropy. Obviously, if magnetic carriers occur along both bedding and cleavage, as in the present study, these can be considered as natural examples of two magnetic fabrics (cf. Housen *et al.* 1993). Our data confirm the results of Housen *et al.* (1993) in the way that the shape parameter changes with the angle between cleavage and bedding, resulting in prolate ellipsoids in the case of high cleavage/bedding angles and oblate ellipsoids in the case of small cleavage/bedding angles. Seemingly in contrast with this, Parés & van der Pluijm (2003) deduce a direct relationship between the magnetic susceptibility shape parameter and tectonic shortening in rocks having a very weakly developed cleavage (pencil structure). However, by definition, this link seems questionable, considering that the 'tectonic shortening', based on the length-to-width ratios of pencil structures, is related to the incipient cleavage (at high angles to bedding), whereas all minimum susceptibility axes are perpendicular to bedding, thus reflecting a compaction strain rather than a tectonic shortening strain.

The demonstrated influence of the cleavage/bedding angle on the shape of the susceptibility ellipsoid seemingly resembles the influence of pre-deformation compaction strain (bedding-parallel fabric) and position within a fold (large cleavage/bedding angle in hinge, small angles in limbs) on the shape and the orientation of the finite strain ellipsoid in structural geology. Finite strains are not only controlled by the incremental strain during deformation (related to cleavage development), but are also controlled by the pre-deformation compaction strains (Sanderson 1976; Maltman 1981; Ramsay & Huber 1983; Paterson *et al.* 1995). Depending on the folding mechanism and relative degree of pre-deformation compaction, this can lead to prolate finite strains in the fold hinge zones (large cleavage/bedding angles) and oblate finite strains in the fold limbs (small cleavage/bedding angles; cf. change in strain ellipsoid across a flexural fold). As we have observed in the Ronquières section (Debacker 1996; Debacker *et al.* 1999), the shape of calcitic nodules changes around the folds with changing cleavage/bedding angles, resulting in prolate nodules in the fold hinges (large cleavage/bedding angle) and 'plane strain' to oblate nodules in the fold limbs (small cleavage/bedding angles). However, a similar relationship between magnetic susceptibility shape parameter and cleavage/bedding angle is hardly ever documented in natural rocks (cf. Gil-Imaz *et al.* 2000). Lüneburg *et al.* (1999) noticed a change in finite strain from oblate to plane strain, going from a fold limb to a fold hinge, but did not document a similar change in magnetic susceptibility shape parameter, nor in phyllosilicate anisotropy. This implies that there is more to controlling the shape of the magnetic susceptibility ellipsoid than the simple superposition of a tectonic strain on a pre-deformation compaction strain (cf. Housen *et al.* 1993; Gil-Imaz *et al.* 2000). Indeed, apart from the degree of preferred orientation of the magnetic carriers, which can be related to strain, the type and the relative concentration of the different magnetic carriers along the fabric elements also control the shape and orientation of the susceptibility ellipsoid (e.g. Borradaile 1987, 1988; Housen *et al.* 1993; cf. Parés & van der Pluijm 2003).

Apart from an increase in shape parameter, Housen *et al.* (1993) also suggest an increase in degree of anisotropy with decreasing cleavage/bedding angle. Although we do observe an increase in degree of anisotropy for the Cambrian samples (Asquempont Member; not enough variation in angle for Ripain Member) and the five samples of the Neoproterozoic turbidites of the Moesian platform, a decrease in degree of anisotropy with decreasing cleavage/bedding angle becomes apparent in the Silurian samples (Vichenet Formation, not enough variation in angle for the Ronquières Formation) (Fig. 6b). This difference in behaviour of the degree of anisotropy with changing cleavage/bedding angle between the Silurian and the Cambrian may possibly be related to the slight difference in overall shape parameter (Fig. 6a). As we have shown, for similar cleavage/bedding angles, the Silurian samples are shifted towards the prolate field with respect to the Cambrian samples (and those of the Moesian platform). This may possibly also be related to the different fields occupied by the Cambrian samples and the Silurian samples on a $T–T_R$ graph (Fig. 12). Housen *et al.* (1993) modelled the effect of the variation in cleavage/bedding angle by means of two differently oriented magnetic fabrics of identical composition (magnetite, with variable concentrations). In real rocks, however, the two differently oriented fabrics are not likely to have the same mineralogical composition. In our examples, the shape and degree of anisotropy of the AMS-ellipsoid of the Asquempont Member, which complies with the trend modelled by Housen *et al.* (1993), are controlled by mica oriented along the cleavage plane on the one hand, and chlorite and ferromagnetic carriers (magnetite) oriented along the bedding plane on the other hand (Fig. 15). In contrast, in the case of the Vichenet Formation, the shape and the degree of anisotropy of the AMS ellipsoid are controlled by mica, matrix-chlorite and ferromagnetic carriers (pyrrhotite) oriented along the cleavage plane on the one hand, and another carrier, probably paramagnetic and presumably large, Fe-rich chlorite, oriented along the bedding plane on the other hand (Fig. 15). This difference in relative orientation of magnetic (*s.l.*) mineralogy may well be the cause of the different behaviour of degree of anisotropy with respect to changes in cleavage/bedding angle (Fig. 6b), the tendency for the Silurian samples to show a slight shift towards the prolate field with respect to the Cambrian samples for similar cleavage/bedding angles (Fig. 6a) and the fact that the Cambrian samples and the Silurian samples occupy different fields on a $T–T_R$ graph (Fig. 12). If such is the case, then obviously AMS cannot be used as a strain gauge in deformed sedimentary rocks, characterized by two magnetic fabrics, the first one being a bedding-parallel compaction fabric and the second one being a cleavage-parallel tectonic fabric.

Conclusion

On the basis of experiments and numerical models, Housen *et al.* (1993) gave an outline of the characteristics of composite magnetic anisotropy fabrics, caused by the presence of two orientation populations of magnetic (*s.l.*) carriers. The present study, performed on low-grade, weakly to moderately deformed, fine-grained sedimentary rocks from the Brabant Massif, characterized by a bedding fabric and a moderately developed cleavage fabric (embryonic cleavage stage to cleavage stage of Ramsay & Huber 1983) complements the results of Housen *et al.* (1993).

A strong relationship is observed between the angle between cleavage and bedding and the magnetic susceptibility shape parameter (T). High angles between cleavage and bedding (e.g. fold hinges) give rise to prolate susceptibility ellipsoids and small angles between cleavage and bedding (e.g. fold limbs) give rise to oblate susceptibility ellipsoids. Importantly, a difference is observed between Cambrian samples and Silurian samples: for similar cleavage/bedding angles the former show a shift towards the oblate field with respect to the latter. Although Housen *et al.* (1993) conclude an increase in degree of anisotropy with decreasing cleavage/bedding angle, we observe an increase with decreasing cleavage/bedding angle for the Cambrian samples, but a decrease with decreasing cleavage/bedding angle for the Silurian samples. Furthermore, a difference between the Cambrian and Silurian samples is also observed on a $T–T_R$ graph. The differences in shape parameter for similar cleavage/bedding angles, the different behaviour of the degree of anisotropy with decreasing cleavage/bedding angle and the different position on a $T–T_R$ graph of the Cambrian samples with respect to the Silurian samples are all tentatively attributed to differences in magnetic mineralogy and relative orientation and concentration of the different magnetic (*s.l.*) carriers.

In the light of the present observations, we suggest, like Housen *et al.* (1993), that AMS, although being a measure of petrofabric anisotropy, cannot be used as a strain gauge in rocks having composite magnetic anisotropy fabrics (cf. Borradaile 1988, 1991). Considering the mineralogical composition of low-grade, pelitic rocks and taking into account the influence of a large number of factors on the presence, concentration and relative orientation of paramagnetic (phyllosilicates) and ferromagnetic minerals (relative degree of tectonic shortening and compaction, degree of metamorphism, relative timing between metamorphism and deformation, sediment source/composition, fluid composition during and after diagenesis, metamorphism and deformation; cf. Rochette 1987*b*; Borradaile 1987; Robion *et al.* 1999), it becomes clear that in weakly to moderately deformed, cleaved, low-grade pelitic rocks, composite magnetic anisotropy fabrics are likely to occur. In such cases, AMS will generally not reflect finite strain, either qualitatively or quantitatively. Only in very specific cases, in which AMS is effectively controlled by one orientation population of magnetic (*s.l.*) carriers parallel to one of the fabric elements (cleavage or bedding), can one consider the possibility to link AMS to finite strain. Examples of specific cases are the two end members of deformed pelitic rocks, being undeformed rocks which only underwent compaction (shales), on the one hand, and intensely deformed rocks in which the initial bedding fabric is completely destroyed (slates, schists), on the other hand. It is suggested that when applying AMS to deformed pelitic rocks, special attention should be paid to the relationship between the maximum (K1) and minimum (K3) susceptibility axis on the one hand and the macroscopic fabric elements on the other hand (cf. Rochette *et al.* 1992). If K1 coincides with the cleavage/bedding intersection and a mismatch occurs between K3 and the pole to bedding and cleavage, then AMS is unlikely to record finite strain (cf. Housen *et al.* 1993).

We are grateful to A. Seghedi for guiding us to outcrops of the Neoproterozoic turbidites of the Moesian platform (Dobrogea, Romania). We kindly acknowledge K. Ullemeyer, J. M. Parés and F. Martín-Hernández for the very constructive remarks. T. Debacker is a Postdoctoral Fellow of the F.W.O.-Vlaanderen. M. Sintubin is a Research Associate of the Onderzoeksfonds K.U.Leuven. This work forms part of research project G.0094.01 of the F.W.O.-Vlaanderen. The research in Romania benefits from the International scientific and technological cooperation program from the Science, Innovation and Media Department of the Ministry of the Flemish Community (BIL01/34).

References

Aubourg, C., Rochette, P. & Vialon, P. 1991. Subtle stretching lineation revealed by magnetic fabric of Callovian-Oxfordian black shales (French Alps). *Tectonophysics*, **185**, 211–223.

Belmans, M. 2000. *Structurele geologie van het Siluur uit de Orneauvallei, Massief van Brabant*. M.Sc. thesis, Laboratorium voor Paleontologie, Universiteit Gent.

Borradaile, G. J. 1987. Anisotropy of magnetic susceptibility: rock composition versus strain. *Tectonophysics*, **138**, 327–329.

Borradaile, G. J. 1988. Magnetic susceptibility, petrofabrics and strain – a review. *Tectonophysics*, **156**, 1–20.

Borradaile, G. J. 1991. Correlation of strain with anisotropy of magnetic susceptibility (AMS). *PAGEOPH*, **135**, 15–29.

Borradaile, G. J. & Henry, B. 1997. Tectonic applications of magnetic susceptibility and its anisotropy. *Earth-Science Reviews* **42**, 49–93.

Borradaile, G. J. & Tarling, D. H. 1981. The influence of deformation mechanisms on magnetic fabrics in weakly deformed rocks. *Tectonophysics*, **77**, 151–168.

Borradaile, G. J. & Werner, T. 1994. Magnetic anisotropy of some phyllosilicates. *Tectonophysics*, **235**, 223–248.

Bouma, A. H. 1962. *Sedimentology of Some Flysch Deposits*. Amsterdam: Elsevier.

Debacker, T. N. 1996. *Structureel-geologische studie van Siluur-afzettingen te Ronquières, Massief van Brabant*. M.Sc. thesis, Laboratorium voor paleontologie, Universiteit Gent.

DEBACKER, T. N. 2001. *Palaeozoic deformation of the Brabant Massif within eastern Avalonia: how, when and why?* Ph.D. thesis, Laboratorium voor paleontologie, Universiteit Gent.

DEBACKER, T. N., SINTUBIN, M. & VERNIERS, J. 1999. Cleavage/fold relationships in the Silurian metapelites, southeastern Anglo-Brabant fold belt (Ronquières, Belgium). *Geologie & Mijnbouw*, **78**, 47–56.

DEBACKER, T. N., SINTUBIN, M. & VERNIERS, J. 2002. Timing and duration of the progressive deformation of the Brabant Massif, Belgium. *Aardkundige Mededelingen*, **12**, 73–76.

DEBACKER, T. N., SINTUBIN, M. & VERNIERS, J. 2004. Transitional geometries between gently plunging and steeply plunging folds – an example from the Lower Palaeozoic Brabant Massif, Anglo-Brabant fold belt, Belgium. *Journal of the Geological Society, London*, **161**, 641–652.

DE SCHEPPER, S. 2000. *Kartering, lithostratigrafie en biostratigrafie met Chitinozoa van de Siluurtypesecties van de Orneauvallei (Massief van Brabant)*. M.Sc. thesis, Laboratorium voor Paleontologie, Universiteit Gent.

DE VOS, W., VERNIERS, J., HERBOSCH, A. & VANGUESTAINE, M. 1993. A new geological map of the Brabant Massif, Belgium. *Geological Magazine*, **130**, 605–611.

FRIZON DE LAMOTTE, D., SOUQUÉ, C., GRELAUD, S. & ROBION, P. 2002. Early record of tectonic magnetic fabric during inversion of a sedimentary basin: examples from the Corbières transfer zone. *Bulletin de la Société Géologique de France*, **173**, 461–469.

FULLER, M. D. 1964. On the magnetic fabric of certain rocks. *Journal of Geology*, **72**, 368–376.

GIL-IMAZ, A., POCOVI, A., LAGO, M. & PARÉS, J. M. 2000. Effect of lithostatic pressure and tectonic deformation on the magnetic fabric (anisotropy of magnetic susceptibility) in low-grade metamorphic rocks. *Journal of Geophysical Research*, **105**, 21305–21317.

GEERKENS, B. & LADURON, D. 1996. *Etude du métamorphisme du Massif du Brabant*. Unpublished BNRE-report.

GRAHAM, J. W. 1954. Magnetic susceptibility anisotropy, an unexploited petrofabric element. *Bulletin of the Geological Society of America*, **65**, 1257–1258.

HERBOSCH, A., VERNIERS, J., DEBACKER, T. N., BILLIAERT, B., DE SCHEPPER, S. & BELMANS, M. 2002. The Lower Palaeozoic stratigraphy and sedimentology of the Brabant Massif in the Dyle and Orneau valleys and of the Condroz Inlier at Fosses: an excursion guidebook. *Geologica Belgica*, **5**, 71–142.

HIRT, A. M., EVANS, K. F. & ENGELDER, T. 1995. Correlation between magnetic anisotropy and fabric for the Devonian shales on the Appalachian Plateau. *Tectonophysics*, **247**, 121–132.

HIRT, A. M., JULIVERT, M. & SOLDEVILA, J. 2000. Magnetic fabric and deformation in the Navia-Alto Sil slate belt, northwestern Spain. *Tectonophysics*, **320**, 1–16.

HO, N.-C., PEACOR, R. & VAN DER PLUIJM, B. A. 1995. Reorientation mechanisms of phyllosilicates in the mudstone-to-slate transition at Lehigh Gap, Pennsylvania. *Journal of Structural Geology*, **17**, 345–356.

HOUSEN, B. A., RICHTER, C. & VAN DER PLUIJM, B. A. 1993. Composite magnetic anisotropy fabrics: experiments, numerical models, and implications for the quantification of rock fabrics. *Tectonophysics*, **220**, 1–12.

HROUDA, F. 1982. Magnetic anisotropy of rocks and its application in geology and geophysics. *Geophysical Surveys*, **5**, 37–82.

HROUDA, F. 2002. The use of anisotropy of magnetic remanence in the resolution of the anisotropy of magnetic susceptibility into its ferromagnetic and paramagnetic components. *Tectonophysics*, **347**, 269–281.

HROUDA, F. & JELÍNEK, V. 1990. Resolution of ferromagnetic and paramagnetic anisotropies, using combined low-field and high-field measurements. *Geophysical Journal*, **103**, 75–84.

JACKSON, M. 1991. Anisotropy of magnetic remanence: a brief review of mineralogical sources, physical origins, and geological applications, and comparison with susceptibility anisotropy. *PAGEOPH*, **136**, 1–28.

JACKSON, M., GRUBER, W., MARVIN, J. & BANERJEE, S. K. 1988. Partial anhysteretic remanence and its anisotropy: applications and grainsize-dependence. *Geophysical Research Letters*, **15**, 440–443.

JELÍNEK, V. 1981. Characterisation of the magnetic fabric of rocks. *Tectonophysics*, **79**, 63–67.

JELÍNEK, V. 1993. Theory and measurement of the anisotropy of isothermal remanent magnetisation of rocks. *Travaux Géophysiques*, **37**, 124–134.

JELÍNEK, V. & POKORNÝ, J. 1997. Some new concepts in the technology of transformer bridges for measuring susceptibility anisotropy of rocks. *Physics and Chemistry of the Earth*, **22**, 179–181.

LEGRAND, R. 1967. Ronquières, documents géologiques. *Mémoire pour servir à l'Explication des Cartes géologiques et minières de la Belgique*, **6**, 1–60.

LI, Z. X. & POWELL, C. MCA. 1993. Magnetic fabric in mid-Cambrian rocks of the Central Flinders Zone and implications for the regional tectonic history. *Tectonophysics*, **223**, 165–176.

LOUWYE, S., VAN GROOTEL, G. & VERNIERS, J. 1992. The stratigraphy of the type locality of the ?late Wenlock/early Ludlow Mont Godart Formation and the early Ludlow Ronquières Formation, Brabant Massif, Belgium. *Annales de la Société Géologique de Belgique*, **115**, 307–331.

LOWRIE, W. 1990. Identification of ferromagnetic minerals in a rock by coercivity and unblocking temperature properties. *Geophysical Research Letters* **17**, 159–162.

LÜNEBURG, C. M., LAMPERT, S. A., LEBIT, H. D., HIRT, A. H., CASEY, M. & LOWRIE, W. 1999. Magnetic anisotropy, rock fabrics and finite strain in deformed sediments of SW Sardinia (Italy). *Tectonophysics* **307**, 51–74.

MALTMAN, A. J. 1981. Primary bedding-parallel fabrics in structural geology. *Journal of the Geological Society, London*, **138**, 475–483.

MARTÍN-HERNÁNDEZ, F. & HIRT, A. M. 2003. The anisotropy of magnetic susceptibility in biotite, muscovite and chlorite single-crystals. *Tectonophysics*, **367**, 13–28.

MCCABE, C., JACKSON, M. & ELLWOOD, B. B. 1985. Magnetic anisotropy in the Trenton Limestone: results of a new technique, anisotropy of anhysteretic susceptibility. *Geophysical Research Letters*, **12**, 333–336.

NAKAMURA, N. & BORRADAILE, G. 2001. Do reduction spots predate finite strain? A magnetic diagnosis of Cambrian slates in North Wales. *Tectonophysics*, **340**, 133–139.

OERTEL, G. 1983. The relationship of strain and preferred orientation of phyllosilicate grains in rocks-a review. *Tectonophysics*, **100**, 413–447.

PARÉS, J. M. & VAN DER PLUIJM, B. A. 2002. Evaluating magnetic lineations (AMS) in deformed rocks. *Tectonophysics*, **350**, 283–298.

PARÉS, J. M. & VAN DER PLUIJM, B. A. 2003. Magnetic fabrics and strain in pencil structures of the Knobs Formation, Valley and Ridge Province, US Appalachians. *Journal of Structural Geology*, **25**, 1349–1358.

PATERSON, S. R., YU, H. & OERTEL, G. 1995. Primary and tectonic fabric intensities in mudrocks. *Tectonophysics*, **247**, 105–119.

PIESSENS, K., VIAENE, W. & MUCHEZ, PH. 2000. *Laboratoriumstudie van Boorkernen in het Massief van Brabant*. Unpublished ANRE-report (report VLA98-3-6), Afdeling Fysico-Chemische Geologie, Katholieke Universiteit Leuven.

RAMSAY, J. G. & HUBER, M. I. 1983. *The techniques of modern structural geology: Volume 1: Strain analysis*. Academic Press, London.

RATHORE, J. S. 1979. Magnetic susceptibility anisotropy in the Cambrian slate belt of North Wales and correlation with strain. *Tectonophysics*, **53**, 83–97.

ROBION, P., FRIZON DE LAMOTTE, D., KISSEL, C. & AUBOURG, C. 1995. Tectonic versus mineralogical contribution to the magnetic fabrics of epimetamorphic slaty rocks: an example from the Ardennes massif (France-Belgium). *Journal of Structural Geology*, **17**, 1111–1124.

ROBION, P., KISSEL, C., FRIZON DE LAMOTTE, D., LORAND, J.-P. & GUÉZOU, J.-C. 1997. Magnetic mineralogy and metamorphic zonation in the Ardennes Massif (France-Belgium). *Tectonophysics*, **271**, 231–248.

ROBION, P., AVERBUCH, O. & SINTUBIN, M. 1999. Fabric development and metamorphic evolution of Lower Palaeozoic slaty rocks from the Rocroi massif (French-Belgian Ardennes): new constraints from magnetic fabrics, phyllosilicate preferred orientation and illite crystallinity data. *Tectonophysics*, **309**, 257–273.

ROCHETTE, P. 1987*a*. Magnetic susceptibility of the rock matrix related to magnetic fabric studies. *Journal of Structural Geology*, **9**, 1015–1020.

ROCHETTE, P. 1987*b*. Metamorphic control of the mineralogy of black shales in the Swiss Alps: towards the use of 'magnetic isograds'. *Earth and Planetary Science Letters*, **84**, 446–456.

ROCHETTE, P., JACKSON, M. & AUBOURG, C. 1992. Rock magnetism and the interpretation of anisotropy of magnetic susceptibility. *Reviews of Geophysics*, **30**, 209–226.

SAINT BÉZAR, B., HÉBERT, R., AUBOURG, C., ROBION, P., SWENNEN, R. & FRIZON DE LAMOTTE, D. 2002. Magnetic fabric and petrographic investigation of hematite-bearing sandstones through ramp-related folds : examples from the South High Atlas front (Morocco). *Journal of Structural Geology*, **24**, 1507–1520.

SANDERSON, D. J. 1976. The superposition of compaction and plane strain. *Tectonophysics*, **30**, 35–54.

SINTUBIN, M. 1994*a*. Phyllosilicate preferred orientation in relation to strain path determination in the Lower Palaeozoic Stavelot-Venn Massif (Ardennes, Belgium). *Tectonophysics*, **237**, 215–231.

SINTUBIN, M. 1994*b*. Textures in shales and slates. *In:* BUNGE, H. J., SIEGENUND, S., SKROTSKI, W. & WEBER, K. (eds) *Textures of Geological Materials*. DGM Informationsgesellschaft Verlag, 221–229.

SINTUBIN, M. 1997. Cleavage-fold relationships in the Lower Paleozoic Brabant Massif (Belgium). *Aardkundige Mededelingen*, **8**, 161–164.

SINTUBIN, M. 1998. Mica (110) pole figures in support of Marchian behaviour of phyllosilicates during the development of phyllosilicate preferred orientation. *Materials Science Forum*, **273–275**, 601–606.

SINTUBIN, M. 1999. Arcuate fold and cleavage patterns in the southeastern part of the Anglo-Brabant Fold Belt (Belgium): tectonic implications. *Tectonophysics*, **309**, 81–97.

SINTUBIN, M., WENK, H.-R. & PHILLIPS, D. S. 1995. Texture development in materials with a platy grain morphology. A comparison between cold pressed Bi2223-powders and experimental and natural phyllosilicate fabrics. *Materials Science and Engineering*, **A202**, 157–171.

SINTUBIN, M., BRODKOM, F. & LADURON, D. 1998. Cleavage-fold relationships in the Lower Cambrian Tubize Group, southeast Anglo-Brabant Fold Belt (Lembeek, Belgium). *Geological Magazine*, **135**, 217–226.

STEPHENSON, A., SADIKUN, S. & POTTER, D. K. 1986. A theoretical and experimental comparison of the anisotropies of magnetic susceptibility and remanence in rocks and minerals. *Geophysical Journal of the Royal Astronomical Society*, **84**, 185–200.

TARLING, D. H. & HROUDA, F. 1993. *The Magnetic Anisotropy of Rocks*. Chapman & Hall, London.

VAN DER PLUIJM, B. A., HO, N.-C. & PEACOR, D. R. 1994. High-resolution X-ray texture goniometry. *Journal of Structural Geology*, **16**, 1029–1032.

VAN GROOTEL, G., VERNIERS, J., GEERKENS, B., LADURON, D., VERHAEREN, M., HERTOGEN, J. & DE VOS, W. 1997. Timing of subsidence-related magmatism, foreland basin development, metamorphism and inversion in the Anglo-Brabant fold belt. *Geological Magazine*, **134**, 607–616.

VERNIERS, J., LOUWYE, S. & VAN GROOTEL G. 1992. Lithostratigraphical descriptions of the Mont Godart and the Ronquières Formations in their type localities and evaluation of the previous descriptions. *Professional Paper of the Geological Survey of Belgium*, **252**, 1–67.

VERNIERS, J., HERBOSCH, A. ET AL., 2001 Cambrian-Ordovician-Silurian lithostratigraphical units (Belgium). *Geologica Belgica*, **4**, 5–38.

VERNIERS, J., PHARAOH, T. ET AL., 2002. The Cambrian to mid Devonian basin development and deformation history of Eastern Avalonia, east of the Midlands Microcraton: new data and a review. In: *Palaeozoic Amalgamation of Central Europe*. Geological Society, London, Special Publications, **201**, 47–93.